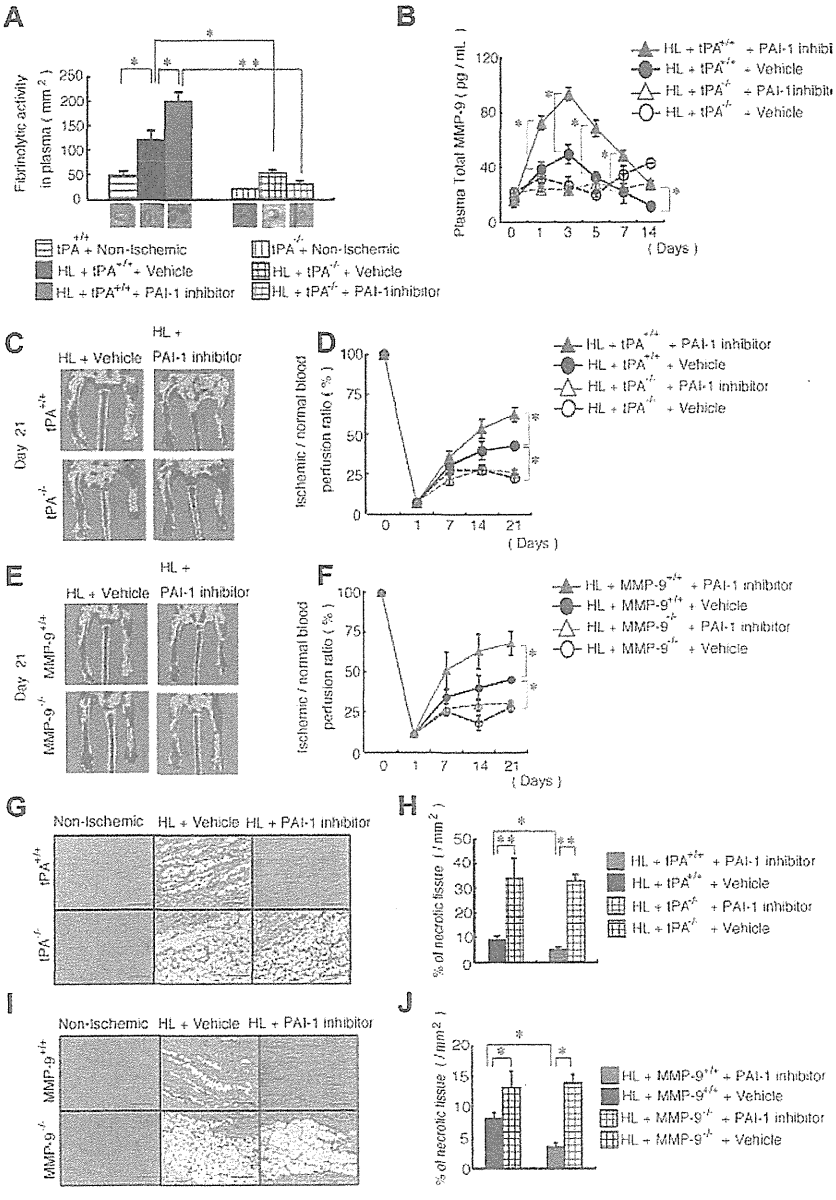

Figure 2. Improved ischemic tissue regeneration after PAI-1 inhibitor treatment depends on tPA and MMP-9. (A-J) HL ischemia was induced in $tPA^{+/+}$, $tPA^{-/-}$, $MMP\text{-}9^{+/+}$, and $MMP\text{-}9^{-/-}$ mice and the mice were then treated with or without PAI-1 inhibitor daily from days 0-6. (A) Fibrinolytic activity in plasma samples of HL-ischemia–induced $tPA^{+/+}$ and $tPA^{-/-}$ mice was analyzed on day 1 using a fibrin plate assay (n = 3/group). (B) MMP-9 plasma levels were determined in $tPA^{+/+}$ and $tPA^{-/-}$ mice treated with the PAI-1 inhibitor or with vehicle by ELISA (n = 9 for $tPA^{+/+}$ mice; n = 3 for $tPA^{-/-}$ mice). (C,E) Representative images of limb perfusion analyzed using a laser Doppler. (D,F) The limb perfusion ratio (ischemic/nonischemic) over time of $tPA^{+/+}$ and $tPA^{-/-}$ mice (D) and $MMP\text{-}9^{+/+}$ and $MMP\text{-}9^{-/-}$ mice (F) treated with the PAI-1 inhibitor or with vehicle (n = 3/group). (G-J) Necrotic areas in sections of H&E-stained muscle sections (G,I) from untreated and PAI-1 inhibitor-treated ischemic limbs (scale bars, 200 mm). (H,J) Necrotic areas in ischemic muscle tissue sections were evaluated after 21 days (n = 3/group). Data represent means ± SEM. $^*P < .05$; $^{**}P < .01$.

HL-ischemia–induced $tPA^{-/-}$ mice treated with vehicle or with the PAI-1 inhibitor (Figure 2B).

We next determined whether endogenous tPA and MMP-9 mediate the improved tissue regeneration that is observed after PAI-1 inhibitor treatment. Indeed, PAI-1 inhibitor treatment resulted in faster blood flow recovery in the ischemic limbs of wild-type mice compared with vehicle-treated wild-type mice, but such enhancement was not observed in $tPA^{-/-}$ mice or $MMP\text{-}9^{-/-}$ mice (Figure 2C-F). Ischemic tissue sections from PAI-1 inhibitor-treated $tPA^{-/-}$ and $MMP\text{-}9^{-/-}$ mice showed vast areas of necrotic tissue compared with PAI-1 inhibitor-treated $tPA^{+/+}$ and $MMP\text{-}9^{+/+}$ mice (Figure 2G-J). These data indicate that endogenous tPA and MMP-9 are required for the tissue-regeneration-promoting effects of PAI-1 inhibition.

PAI-1 inhibition improves tPA-dependent ischemic revascularization

PAI-1 inhibitor treatment resulted in faster collateral vessel growth, which was observed macroscopically (Figure 3A) and microscopically after VWF staining in the ischemic limb of C57BL/6 mice (Figure 3B) and in the ischemic limb of $tPA^{+/+}$ mice compared with vehicle-treated mice (Figure 3C-D), but did not show such enhancement in the ischemic limb of $tPA^{-/-}$ mice. We have shown previously that tPA treatment increases VEGF-A plasma levels and that tPA administration can promote myeloid-cell expansion by MMP-9–mediated release of KitL from stromal/niche cells.[19] Indeed, augmented plasma levels of VEGF-A (Figure 3E) and KitL (Figure 3F) were found in PAI-1 inhibitor-treated HL-ischemic $tPA^{+/+}$ mice, but not in PAI-1 inhibitor-treated HL-ischemic $tPA^{-/-}$ mice. Furthermore, G-CSF, a cytokine known to stimulate BM granulopoiesis, was also increased after PAI-1 inhibitor treatment in HL-ischemic mice in a MMP-9– and tPA-dependent manner (Figure 3G-H). In addition, recombinant tPA administration augmented G-CSF serum levels in normoxic C57BL/6 mice (Figure 3I). These data indicate that PAI-1 inhibition during ischemic recovery augments both angiogenic and hematopoietic factors.

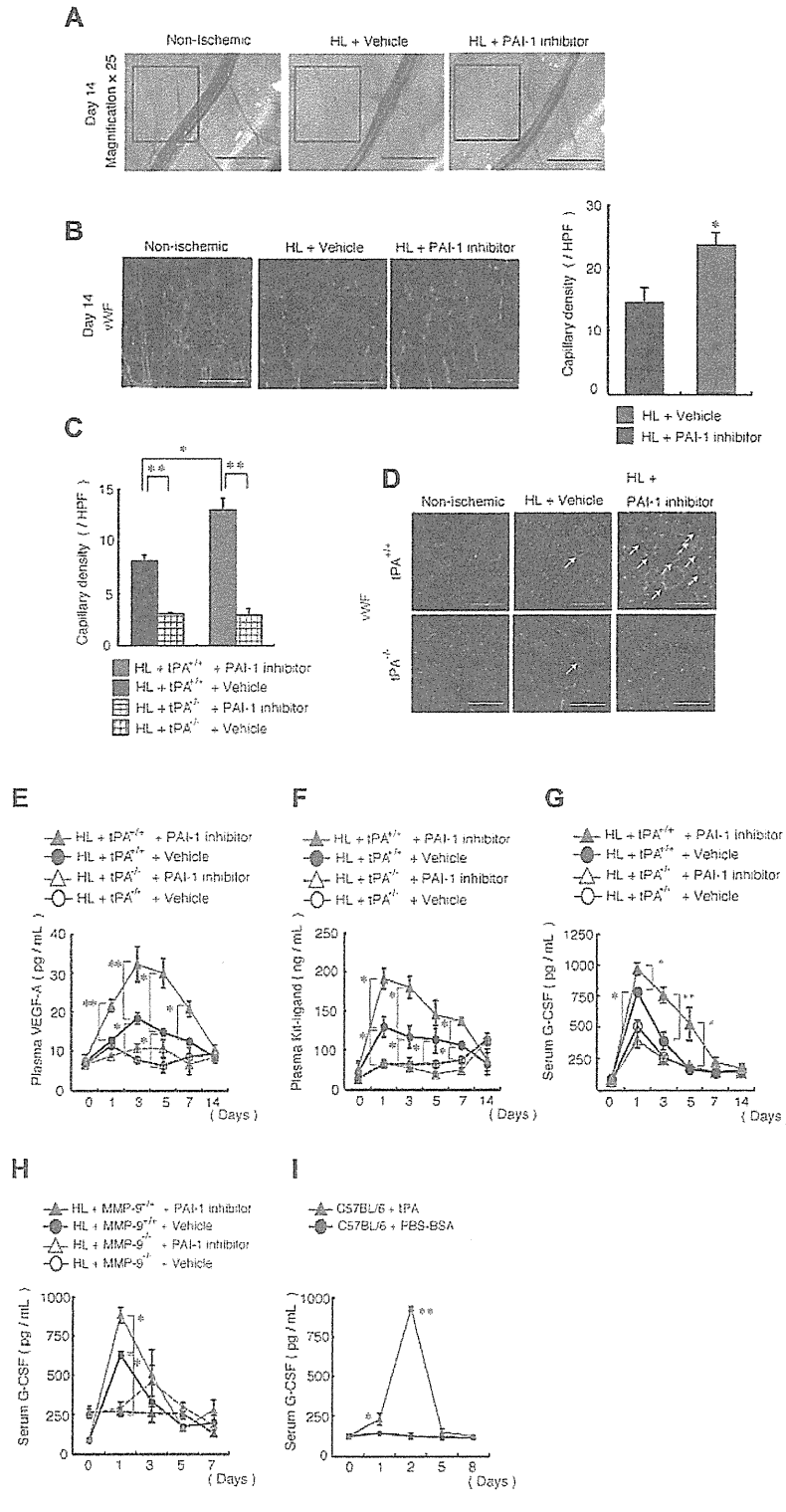

Figure 3. In vivo blockade of PAI-1 augments neoangiogenesis and growth factor release. (A) Macroscopic images of the lower limb region of nonischemic and PAI-1 inhibitor- or vehicle-treated wild-type mice were captured on day 14 after HL ischemia induction (magnification, 25×; scale bars, 2000 mm). The insert box depicts areas of neoangiogenesis. (B-G) HL ischemia was induced in C57BL/6, $tPA^{+/+}$, and $tPA^{-/-}$ mice, and the mice were then treated with or without PAI-1 inhibitor daily from days 0-6. (B-C) Capillary density was measured in sections of the hamstring (B) and adductor muscles (C) based on immunohistochemical staining of VWF per high power field (HPF). (B,D) Representative images of anti-VWF mAb immunohistochemical staining of ischemic muscle sections from HL-ischemia–induced C57BL/6, $tPA^{+/+}$, and $tPA^{-/-}$ mice either left untreated or treated with or without the PAI-1 inhibitor (n = 6/group) analyzed on day 14 after the procedure (scale bars, 200 mm). Arrows depict VWF^{+} capillaries. (E-G) Plasma levels of VEGF-A (E) and KitL (F) and serum levels of G-CSF (G) in HL-ischemia–induced $tPA^{+/+}$ and $tPA^{-/-}$ mice treated with or without PAI-1 inhibitor were determined by ELISA (for VEGF-A, n = 9 for $tPA^{+/+}$ mice and n = 3 for $tPA^{-/-}$ mice; for KitL and G-CSF, n = 7 for $tPA^{+/+}$ mice and n = 3 for $tPA^{-/-}$ mice; for KitL, n = 3 for G-CSF). (H) G-CSF serum levels were analyzed by ELISA in HL-ischemia–induced $MMP\text{-}9^{+/+}$ and $MMP\text{-}9^{-/-}$ mice treated with or without PAI-1 inhibitor (H) and in C57BL/6 mice treated with a serpin-resistant tPA mutant (n = 4-5/group). Values represent the means ± SEM. $^{*}P < .05$; $^{**}P < .001$.

PAI-1 inhibition mobilizes neutrophils into the circulation and promotes neutrophil recruitment into ischemic tissues in vivo

The PAI-1 inhibitor-mediated increase in hematopoietic cytokines prompted us to examine whether the inflammatory response during ischemic recovery might be altered after PAI-1 inhibition. Isolation of leukocytes from ischemic muscle tissues, followed by MACS separation using the anti–Gr-1 Ab, revealed that approximately 40% of infiltrating leukocytes were neutrophils on day 5 of HL ischemia (Figure 4A). PAI-1 inhibitor treatment increased the number of $Gr\text{-}1^{+}$ neutrophils in ischemic sections of $tPA^{+/+}$ mice, but not in $tPA^{-/-}$ mice, compared with vehicle-treated mice (Figure 4B-C).

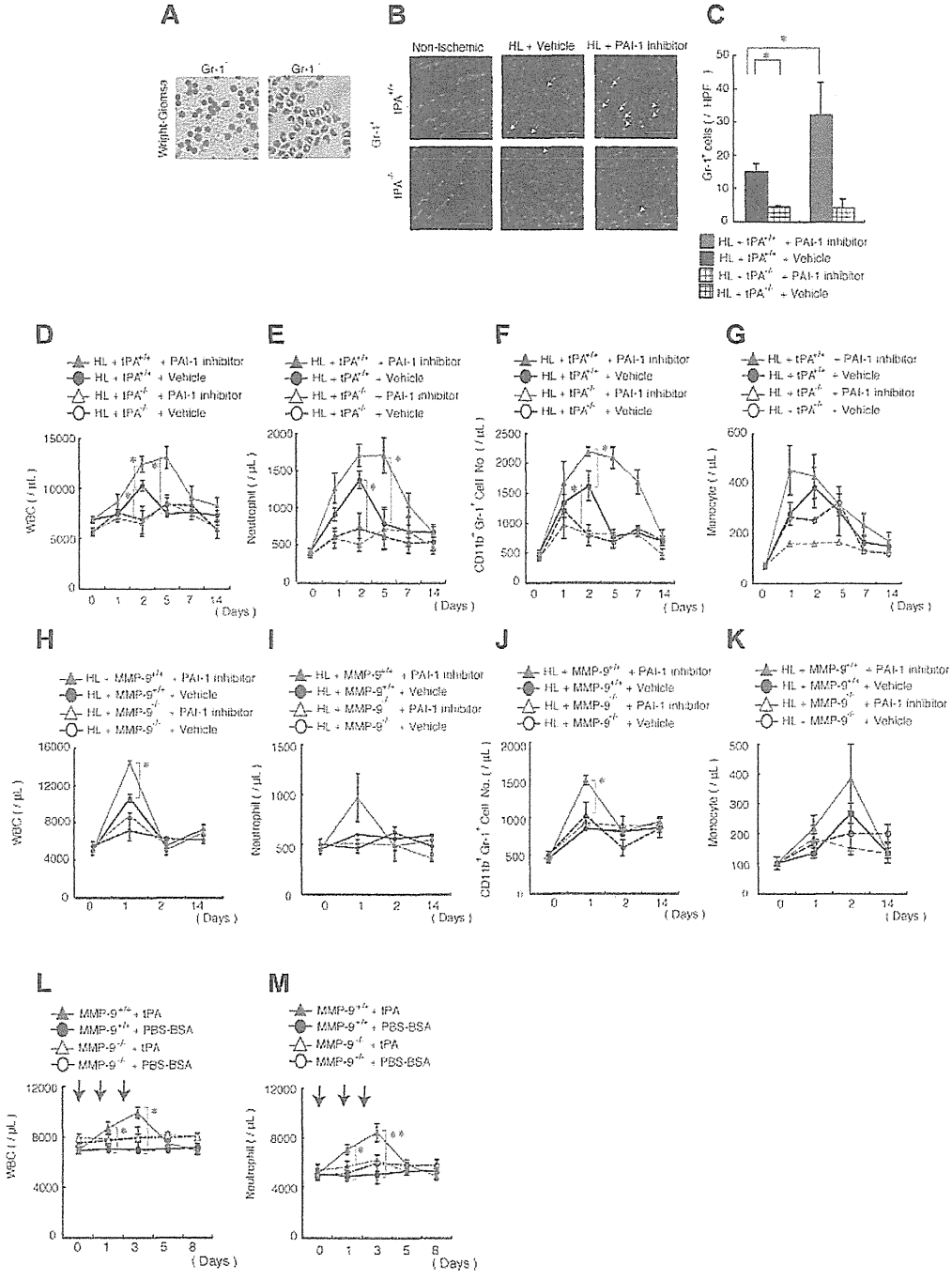

Figure 4. Pharmacologic PAI inhibition mobilizes neutrophils into the circulation and improves their tissue infiltration, a process dependent on endogenous tPA and MMP-9. (A) Wright-Giemsa staining of MACS-isolated infiltrating Gr-1$^+$ and Gr-1$^-$ cells derived from ischemic tissues of C57BL/6 mice on day 5 after HL induction. (B) Immunofluorescent staining of Gr-1 was performed on nonischemic muscle tissues or on HL-ischemic muscle tissues derived from vehicle- or PAI-1 inhibitor-treated HL-ischemic tPA$^{+/+}$ and tPA$^{-/-}$ mice 14 days after the HL procedure. PAI-1 inhibitor was administered daily on days 0-6 after the procedure. The arrows indicate Gr-1$^+$ cells (scale bars, 200 mm). Nuclei were counterstained with DAPI (blue). (C) Quantification of Gr-1$^+$ cells in ischemic muscle tissues (n = 3/group). (D-K) The total number of WBCs (D,H) and the number of neutrophils (E,I), CD11b$^+$Gr-1$^+$ cells (F,J), and monocytes (G,K) were determined in the peripheral blood of PAI-1 inhibitor-treated or vehicle-treated tPA$^{+/+}$ and tPA$^{-/-}$ mice (for B-G, n = 4) and in MMP-9$^{+/+}$ and MMP-9$^{-/-}$ mice (for H-K, n = 6) by counting (D,E,G,H,I,K) or by FACS analysis (F,J). (L-M) The total number of WBCs (L) and neutrophils (M) were counted in in MMP-9$^{+/+}$ and MMP-9$^{-/-}$ mice (n = 4). *$P < .05$; **$P < .001$ for recombinant tPA-treated versus vehicle-treated C57BL/6 mice. Values represent the means ± SEM. Data are expressed as the absolute number of each cell type per milliliter of blood. *$P < .05$.

We next analyzed blood samples to determine whether the augmented neutrophil influx in ischemic tissues was due to an overall increase in circulating blood cells. PAI-1 inhibitor-treated HL-ischemic tPA$^{+/+}$ mice, but not tPA$^{-/-}$ mice, showed an increase in the number of WBCs, including neutrophils, as determined by cell counting and FACS analysis using Abs against CD11b and Gr-1 (Figure 4D-F), but not monocytes, compared with vehicle-treated animals (Figure 4G). MMP-9 deficiency prevented the leukocyte and neutrophil increase, but not the monocyte increase, caused by PAI-1 inhibitor treatment (Figure 4H-K), indicating that PAI-1 inhibitor-mediated neutrophilia was dependent on endogenous MMP-9. Administration of recombinant tPA

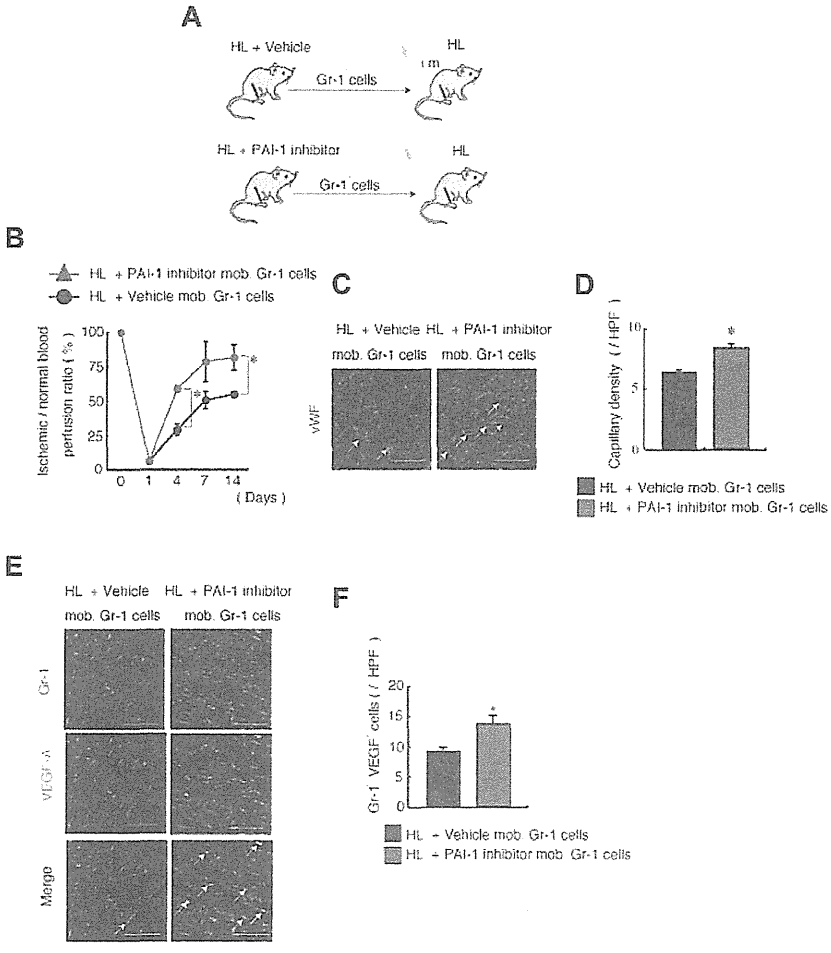

Figure 5. Adoptive transfer of Gr-1$^+$ cells from PAI-1 inhibitor-treated mice improves neoangiogenesis. (A-F) Muscle-derived Gr-1$^+$ cells isolated from HL-ischemia–induced-C57BL/6 donors treated with/without PAI-1 inhibitor were transplanted into HL-ischemia–induced recipients for 3 days (n = 6/group). (A) Experimental scheme of the muscle-derived Gr-1$^+$ cell transplantation assay. (B) Blood flow was determined after transplantation of PAI-1 inhibitor-mobilized versus vehicle-mobilized (mob.) Gr-1$^+$ cells in HL-ischemic C57BL/6 recipients. (C) VWF immunostaining of lower limb ischemic tissue of mice receiving vehicle- or PAI-1 inhibitor-mobilized cell transplantations. Arrows indicate capillaries. Nuclei were counterstained with DAPI (blue staining). Scale bars indicate 200 mm. (D) Capillary density was evaluated per high-power field (HPF). (E) Immunofluorescent staining of Gr-1 and VEGF-A was performed on sections derived from vehicle or PAI-1 inhibitor-mobilized Gr-1 cell-transplanted mice. The arrows indicate transplanted Gr-1$^+$ cells costained with VEGF-A in ischemic tissues. Nuclei were counterstained with DAPI (blue). (F) Quantification of Gr-1$^+$ VEGF-1$^+$ cells under a HPF. Data represent means ± SEM. $^*P < .05$.

induced neutrophilia and, similar to PAI-1 inhibitor administration, this process required endogenous MMP-9 (Figure 4L-M). Therefore, PAI-1 inhibitor treatment not only augmented the absolute number of circulating Gr-1$^+$ cells/neutrophils, but also improved their incorporation into ischemic tissues in a tPA- and MMP-9–dependent manner.

Adoptive transfer of Gr-1$^+$ myeloid cells from PAI-1 inhibitor-treated mice improves revascularization after HL ischemia induction

Our data suggested that neutrophils could be the cellular target for PAI-1 inhibitor-induced improved tissue regeneration. We hypothesized that PAI-1 induction during HL ischemia may alter the ability of neutrophils to stimulate angiogenesis. To test this hypothesis, muscle-derived Gr-1$^+$ cells were obtained from HL-ischemia–induced donor mice that had been treated with or without the PAI-1 inhibitor. These Gr-1$^+$ cells were transplanted into HL recipient mice (Figure 5A) by intramuscular injection. In contrast to cells from vehicle-treated mice, Gr-1$^+$ cells isolated from muscle tissues of PAI-1 inhibitor-treated mice accelerated ischemic reperfusion (Figure 5B) and increased capillary density in ischemic tissues of HL-ischemic recipients (Figure 5C-D). We showed that neutrophils release the proangiogenic factor VEGF-A.[21] Consistent with that result, the absolute number of Gr-1$^+$VEGF-1$^+$ cells was higher in ischemic recipient tissues transplanted with Gr-1$^+$ cells from PAI-1–treated mice (Figure 5E-F).

These data indicate that PAI-1 inhibitor-mediated neoangiogenesis is partially driven by a Gr-1$^+$ muscle-residing cell population.

The proangiogenic PAI-1 inhibitor enhances FGF-2 and VEGF-A function/signaling

We reported previously that a serpin-resistant tPA promoted macrophage-mediated angiogenesis.[22] To determine whether PAI-1 inhibition accelerates macrophage recruitment into ischemic tissues, we quantified the number of infiltrating F4/80$^+$ cells 3 days after initiation of HL ischemia. PAI-1 inhibition did not increase the recruitment of macrophages in muscle tissues compared with vehicle treatment (Figure 6A).

To identify the molecular mechanisms underlying the enhanced angiogenesis observed after PAI-1 inhibition, we examined the expression of angiogenesis-related factors in ischemic muscle tissues derived from PAI-1 inhibitor- and vehicle-treated animals. FGF-2 signaling has been associated with neutrophil-mediated angiogenesis[23] and PAI-1 activity.[22] Immunohistochemical analysis of ischemic muscle tissues demonstrated that the number of F4/80$^+$ cells coexpressing FGF-2 or VEGF-A was not significantly different from vehicle- and PAI-1 inhibitor-treated tissues (Figure 6B). In contrast, the number of ischemic tissue-resident Gr-1$^+$ cells coexpressing both FGF-2 and VEGF-A was higher in sections derived from PAI-1 inhibitor-treated mice (Figure 6C).

FGF-2 can signal through syndecan-4 independently of FGF receptors.[22] Therefore, in the present study, we investigated whether

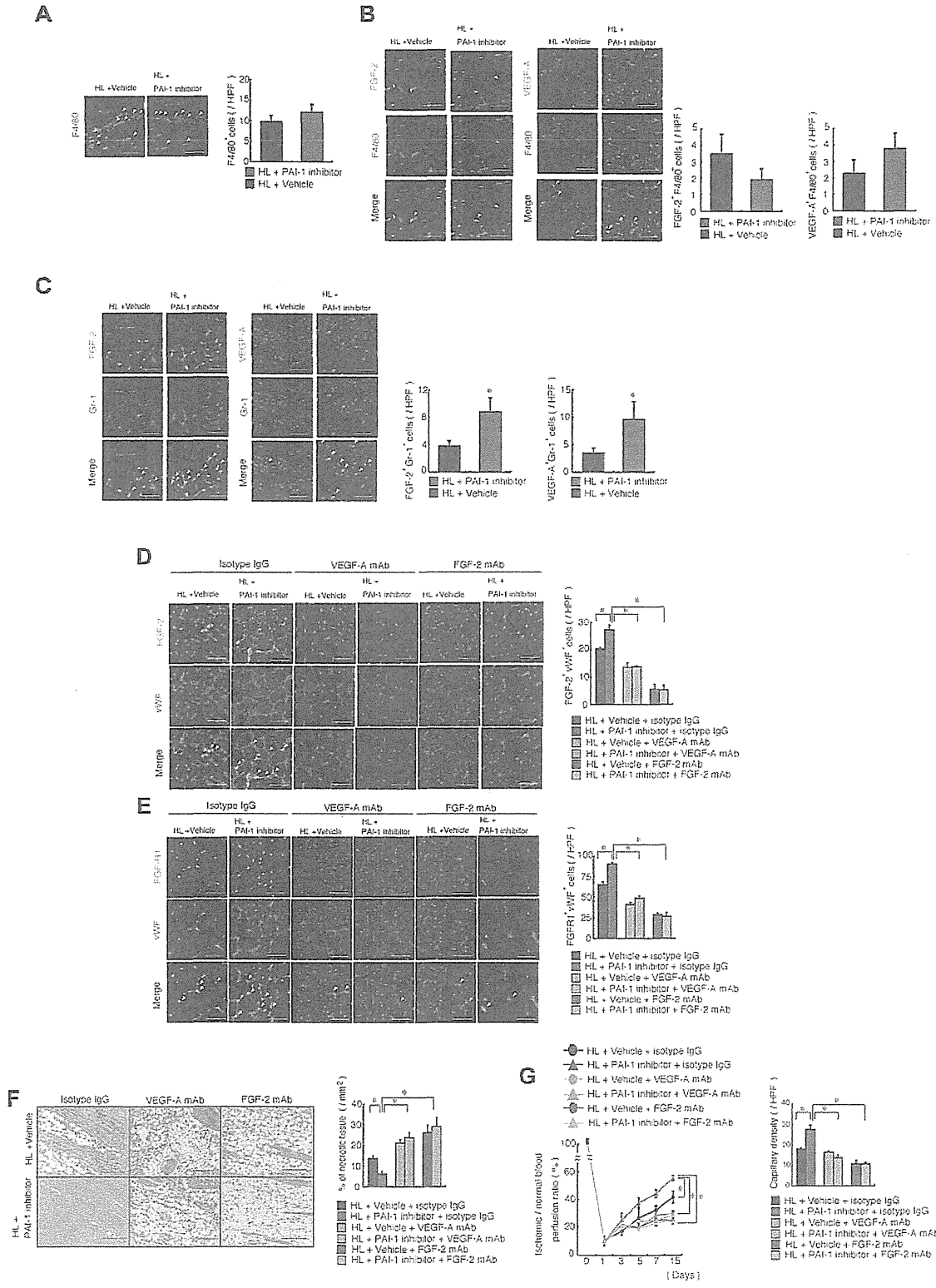

Figure 6. PAI-inhibition induces angiogenesis during HL-ischemic recovery via FGF-2- and VEGF-A–mediated pathways. (A-C) HL-ischemia–induced C57BL/6 mice were treated with the PAI-1 inhibitor or vehicle. Ischemic sections of PAI-1 inhibitor or vehicle-treated mice 3 days after the HL procedure were costained for F4/80 (A), F4/80 and VEGF-A or F4/80 and FGF-2 (B), or Gr-1 and VEGF-A or Gr-1 and FGF-2 (C). Nuclei were counterstained with DAPI (blue). Left panels are representative immunofluorescent images. Arrows indicate VEGF-A$^+$, FGF-2$^+$, F4/80$^+$, or Gr-1$^+$ cells. Right panel shows the quantification of the indicated cell populations per high-power field (HPF; n = 5/group for each experiment). (D-G) HL-ischemia–induced C57BL/6 mice were treated with the PAI-1 inhibitor and coinjected with neutralizing doses of anti–FGF-2, anti–VEGF-A, or anti-IgG control Abs (n = 4/group). (D-E) Ischemic muscle tissues from Ab-treated animals 14 days after the HL procedure were immunofluorescently costained for FGF-2/VWF and FGF-R1/VWF. Nuclei were counterstained with DAPI (blue staining). Arrows indicate FGF-2$^+$/VWF$^+$ and FGF-R1$^+$/VWF$^+$ cells (scale bars, 200 mm). Right panel shows the indicated cell populations quantified per HPF. (F) Left panel, ischemic muscle tissue sections were stained with H&E (scale bars, 200 mm). Right panel shows the quantification of necrotic areas in ischemic H&E-stained tissue sections. (G) Blood flow was determined at the indicated time points. (H) Ischemic muscle tissue sections stained with Abs against VWF antigen on day 14 were used to determine capillary density. Data represent means ± SEM. *$P < .05$.

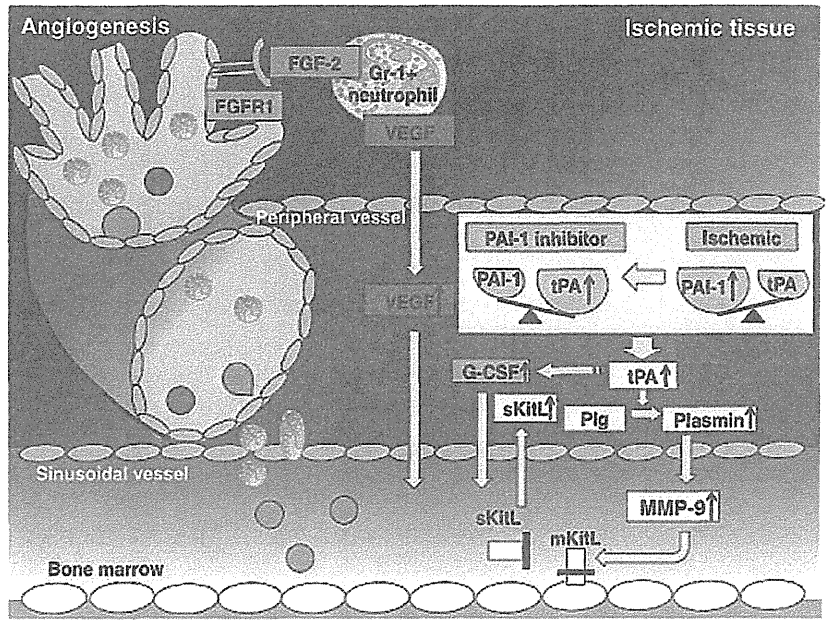

Figure 7. Schematic diagram showing the various molecules involved in the proangiogenic effect of PAI-1 inhibition. Under ischemic conditions, the local balance between the fibrinolytic factor tPA and one of its endogenous inhibitors, PAI-1, is shifted toward a profibrinolytic state with a local increase in tPA. Ischemia systemically results in a profibrinolytic state, a process dependent on endogenous tPA. Pharmacologic PAI-1 inhibition during ischemic recovery improved tissue regeneration due to an expansion of circulating and tissue-resident Gr-1$^+$ neutrophils coexpressing VEGF-A, FGF-2, and TIMP-1–free MMP-9, and to increased release of the angiogenic factor VEGF-A, the hematopoietic growth factor KitL, and G-CSF. Ab neutralization and genetic-knockout studies indicated that both the improved tissue regeneration and the increase in both circulating and ischemic tissue-resident Gr-1$^+$ neutrophils were dependent on the activation of tPA and MMP-9 and on VEGF-A and FGF-2.

expression of FGF-2 or FGFR1 is altered in PAI-1 inhibitor-treated ischemic tissues. Immunohistochemical analysis of ischemic muscle tissue sections revealed that PAI-1 inhibitor treatment augmented FGF-2 and FGF-R1 expression and that this expression colocalized more often to VWF$^+$ cells compared with vehicle-treated controls (Figure 6D-E).

FGF-2–induced angiogenesis requires VEGF signaling.[24] Blockade of VEGF-A and FGF-2 signaling with Abs against murine VEGF-A and FGF-2 inhibited the PAI-1 inhibitor-mediated FGF-2 and FGFR-1 increase on VWF$^+$ cells (Figure 6D-E), as well as the PAI-1 inhibitor-mediated ischemic tissue recovery, and reversed the necrosis-reducing effect of PAI-1 inhibitor treatment (Figure 6F-G) and myeloid cell mobilization (supplemental Figure 1A-C, available on the *Blood* Web site; see the Supplemental Materials link at the top of the online article) in an HL-ischemic model.

Although it is clear that FGF-2–induced angiogenesis requires VEGF signaling,[24] it was unclear whether VEGF-A and FGF-2 signaling are required for PAI-1 inhibitor-mediated tissue neoangiogenesis. Our present data suggest that this might be the case, because VEGF-A and FGF-2 mAb prevented PAI-1 inhibitor-mediated ischemic tissue recovery and neoangiogenesis in an HL-ischemic model (Figure 6F-G).

The results of the present study indicate that the proangiogenic effects observed after PAI-1 inhibitor treatment are mediated by the 2 potent proangiogeneic factors FGF-2 and VEGF-A, and that neutrophils seem to be a source for these growth factors. In addition, both factors were essential for the PAI-1 inhibitor-mediated recruitment of "angiogenic hematopoietic effector cells" into ischemic tissues.

Discussion

The present study identifies activation of the FGF-2 and VEGF-A pathways as the cause of the proangiogeneic effect of drug-induced PAI-1 deficiency in a murine model of HL ischemia. Our data support a mechanism whereby drug-induced PAI-1 inhibition enhances angiogenesis through up-regulation of endogenous tPA and MMP-9. Both proteases are required for neutrophil mobilization and for the release of proangiogenic cytokines, including FGF-2 and VEGF-A (Figure 7). In addition, muscle-infiltrating CD11b$^+$Gr-1$^+$ neutrophils harvested from PAI-1 inhibitor-treated mice coexpressed FGF-2 and VEGF-A and showed an improved capacity to stimulate angiogenesis on adoptive transfer compared with equal numbers of carrier-treated ischemic tissue-derived neutrophils. Ab-blocking experiments revealed that PAI-inhibitor–induced tissue regeneration required FGF-2 and VEGF-A signaling. These data are important for the design of future cell-based therapies, especially in the light of a recent study demonstrating that BM cells harvested from mice with distant ischemia show a reduced capacity to stimulate angiogenesis on adoptive transfer.[25]

FGF family members and its receptors (FGFRs) can promote angiogenesis. In the present study, PAI-1 inhibition-induced augmentation of FGFR1 expression on endothelial cells in ischemic tissues coincided with increased KitL plasma levels. This result is consistent with a previous study showing that FGFR-1–deficient embryoid bodies show decreased expression of KitL.[26] KitL can improve tissue recovery in animal models of HL ischemia.[27-29] Recombinant tPA therapy augments circulating KitL levels[30] and promotes ischemic revascularization.[19] Confirming these data, in the present study, we found that drug-induced PAI-1 inhibition raised KitL plasma levels via tPA augmentation. Our data imply a relationship among the fibrinolytic factors PAI-1/tPA, FGFR1 signaling, and KitL production. However, further studies are required to determine how these pathways interact with each other.

PAI-1 in cooperation with integrins, coagulation, fibrinolysis, and endocytosis has been shown to be important for macrophage migration.[7] In the present study, we show that pharmacologic blockade of PAI-1 increased MMP-9– and tPA-dependent augmentation of tissue-residing neutrophils, but not F4/80$^+$ macrophages, under ischemic conditions. Therefore, PAI-1 seems to act as a negative regulator of neutrophil recruitment during HL-ischemic recovery. Supporting our observations, Renckens et al demonstrated that PAI-1 gene-deficient mice showed an enhanced early influx of neutrophils to the site of inflammation in a murine model of turpentine-induced tissue injury.[31] In this model, no difference

was found between PAI-$1^{-/-}$ and PAI-$1^{+/+}$ mice in factors known to attract neutrophils, including keratinocyte-derived chemokine and macrophage inflammatory protein-2.

Among the factors that can enhance the survival, proliferation, differentiation, and function of neutrophil precursors and mature neutrophils[32] is the hematopoietic growth factor G-CSF. In the present study, we demonstrate for the first time that recombinant tPA and endogenous tPA that is enhanced by PAI-1 inhibition promote the release of G-CSF. G-CSF has been shown to improve tissue recovery in animal models of HL[21] and myocardial[33] and focal cerebral ischemia injuries in both mice and humans[34] by modulating various cell types, including endothelial cells and neutrophils.[21,32] Various studies have demonstrated the importance of MMP-9 for neutrophil-driven neoangiogenesis in an HL-ischemic model.[2,19,21,35] A recent study demonstrated that tissue-infiltrating neutrophil pro-MMP-9 induces angiogenesis catalytically via an FGF-2/FGFR2 pathway.[23] Consistent with that study, we have shown previously that pharmacologic PAI-1 inhibition results in the accumulation of FGF-2– and VEGF-A–expressing Gr-1^{+} neutrophils within ischemic muscle tissues through an effect on endogenous tPA and MMP-9, and in an increase of plasma VEGF-A via up-regulation of endogenous tPA.[19] Neutrophils can secrete tissue inhibitors of metalloproteinase (TIMP)–free MMP-9 that can act in concert with, for example, macrophages to liberate proangiogenic growth factors such as VEGF and FGF-2 that are sequestered to the extracellular matrix.

PAI-1 can inhibit cell adhesion and migration by inhibiting the activity of uPA receptor (uPAR)–bound uPA and by preventing integrin association to vitronectin. Studies with uPAR$^{-/-}$ mice have emphasized the critical role of this receptor in leukocyte trafficking.[31] Indeed, uPAR$^{-/-}$ mice displayed a profoundly reduced neutrophil recruitment to the peritoneal cavity after IP administration of thioglycollate.[36] Our present results are consistent with the findings that neutrophil extravasation into the interstitium after lung ischemia-reperfusion injury after lung transplantation was blocked in tPA-deficient mice.[37] At the molecular level, this blockage was associated with reduced expression of platelet endothelial cell adhesion molecule-1 mediated through the tPA/low-density lipoprotein receptor–related protein/NF-κB signaling pathway.

Reichel et al showed that extravasated plasmin(ogen) mediates neutrophil recruitment in vivo via activation of perivascular mast cells and secondary generation of lipid mediators.[38]

The combined data suggest that strategies aimed at inactivation of PAI-1 (eg, the use of the small-molecule TM5275) could be an immediately clinically applicable therapeutic option for improving angiogenesis in ischemic patients. The results of the present study shed new light on the mechanism by which PAI-1 and tPA enhance neovascularization by modulation of the local and systemic growth factor environment and by alteration of neutrophil migration.

Acknowledgments

The authors thank the FACS core facility at the Institute of Medical Science, University of Tokyo (Tokyo, Japan), for their help.

This work was supported by the Japan Society for the Promotion of Science; Grants-in-Aid for Scientific Research from the Ministry of Education, Culture, Sports, Science and Technology (MEXT; to K.H. and B.H.); a Grant-in-Aid for Scientific Research on Priority Areas from MEXT (to K.H.); the Mitsubishi Pharma Research Foundation (to K.H); a Grant-in-Aid for Scientific Research on Innovative Areas from MEXT (B.H.); the SENSHIN Medical Research Foundation (K.H.); Kyowa Hakko Kirin Co Ltd; the Daiichi Sankyo Company; and by the Program for Improvement of the Research Environment for Young Researchers (to B.H.) funded by the Special Coordination Funds for Promoting Science and Technology of MEXT, Japan.

Authorship

Contribution: Y.T., C.N., and K.S.-K. designed and performed the experiments, analyzed the data, and wrote the manuscript; M.O.-K. and M.I. designed and performed the experiments; A.S., I.G., H.K., and Y.S. developed the analytical tools; T.D., T.M., and Y.T. provided reagents; K.O., K.S., and H.N. provided technical support and conceptual advice; and B.H. and K.H. designed the experiments, analyzed the data, and wrote the manuscript.

Conflict-of-interest disclosure: The authors declare no competing financial interests.

Correspondence: Koichi Hattori, Center for Stem Cell Biology and Regenerative Medicine, Institute of Medical Science, University of Tokyo, 4-6-1, Shirokanedai, Minato-ku, Tokyo 108-8639, Japan; e-mail: khattori@ims.u-tokyo.ac.jp.

References

1. Carmeliet P. Mechanisms of angiogenesis and arteriogenesis. *Nat Med.* 2000;6(4):389.
2. Heissig B, Nishida C, Tashiro Y, et al. Role of neutrophil-derived matrix metalloproteinase-9 in tissue regeneration. *Histol Histopathol.* 2010; 25(6):765-770.
3. Simons M, Ware JA. Therapeutic angiogenesis in cardiovascular disease. *Nat Rev Drug Discov.* 2003;2(11):863-871.
4. Heissig B, Hattori K, Friedrich M, Rafii S, Werb Z. Angiogenesis: vascular remodeling of the extracellular matrix involves metalloproteinases. *Curr Opin Hematol.* 2003;10(2):136-141.
5. Dellas C, Loskutoff DJ. Historical analysis of PAI-1 from its discovery to its potential role in cell motility and disease. *Thromb Haemost.* 2005; 93(4):631-640.
6. Stefansson S, Lawrence DA. The serpin PAI-1 inhibits cell migration by blocking integrin alpha V beta 3 binding to vitronectin. *Nature.* 1996; 383(6599):441-443.
7. Cao C, Lawrence DA, Li Y, et al. Endocytic receptor LRP together with tPA and PAI-1 coordinates Mac-1-dependent macrophage migration. *EMBO J.* 2006;25(9):1860-1870.
8. Carmeliet P, Moons L, Lijnen R, et al. Inhibitory role of plasminogen activator inhibitor-1 in arterial wound healing and neointima formation: a gene targeting and gene transfer study in mice. *Circulation.* 1997;96(9):3180-3191.
9. Fay WP, Shapiro AD, Shih JL, Schleef RR, Ginsburg D. Brief report: complete deficiency of plasminogen-activator inhibitor type 1 due to a frame-shift mutation. *N Engl J Med.* 1992; 327(24):1729-1733.
10. Sawdey MS, Loskutoff DJ. Regulation of murine type 1 plasminogen activator inhibitor gene expression in vivo. Tissue specificity and induction by lipopolysaccharide, tumor necrosis factor-alpha, and transforming growth factor-beta. *J Clin Invest.* 1991;88(4):1346-1353.
11. Sakamoto T, Yasue H, Ogawa H, Misumi I, Masuda T. Association of patency of the infarct-related coronary artery with plasma levels of plasminogen activator inhibitor activity in acute myocardial infarction. *Am J Cardiol.* 1992;70(3):271-276.
12. Juhan-Vague I, Pyke SD, Alessi MC, Jespersen J, Haverkate F, Thompson SG. Fibrinolytic factors and the risk of myocardial infarction or sudden death in patients with angina pectoris. ECAT Study Group. European Concerted Action on Thrombosis and Disabilities. *Circulation.* 1996;94(9):2057-2063.
13. Diebold I, Kraicun D, Bonello S, Gorlach A. The 'PAI-1 paradox' in vascular remodeling. *Thromb Haemost.* 2008;100(6):984-991.
14. Stefansson S, McMahon GA, Petitclerc E, Lawrence DA. Plasminogen activator inhibitor-1 in tumor growth, angiogenesis and vascular remodeling. *Curr Pharm Des.* 2003;9(19):1545-1564.
15. McMahon GA, Petitclerc E, Stefansson S, et al. Plasminogen activator inhibitor-1 regulates tumor growth and angiogenesis. *J Biol Chem.* 2001; 276(36):33964-33968.

16. van Meijer M, Smilde A, Tans G, Nesheim ME, Pannekoek H, Horrevoets AJG. The suicide substrate reaction between plasminogen activator inhibitor 1 and thrombin is regulated by the cofactors vitronectin and heparin. *Blood.* 1997;90(5): 1874-1882.
17. Lijnen HR, Arza B, Van Hoef B, Collen Ds Declerck PJ. Inactivation of plasminogen activator inhibitor-1 by specific proteolysis with stromelysin-1 (MMP-3). *J Biol Chem.* 2000; 275(48):37645-37650.
18. Izuhara Y, Yamaoka N, Kodama H, et al. A novel inhibitor of plasminogen activator inhibitor-1 provides antithrombotic benefits devoid of bleeding effect in non-human primates. *J Cereb Blood Flow Metab.* 2010;30(5):904-912.
19. Ohki M, Ohki Y, Ishihara M, et al. Tissue type plasminogen activator regulates myeloid-cell dependent neoangiogenesis during tissue regeneration. *Blood.* 2010;115(21):4302-4312.
20. Loskutoff DJ, Sawdey M, Keeton M, Schneiderman J. Regulation of PAI-1 gene expression in vivo. *Thromb Haemost.* 1993;70(1): 135-137.
21. Ohki Y, Heissig B, Sato Y, et al. Granulocyte colony-stimulating factor promotes neovascularization by releasing vascular endothelial growth factor from neutrophils. *FASEB J.* 2005;19(14): 2005-2007.
22. Drinane M, Walsh J, Mollmark J, Simons M, Mulligan-Kehoe MJ. The anti-angiogenic activity of rPAI-1(23) inhibits fibroblast growth factor-2 functions. *J Biol Chem.* 2006;281(44):33336-33344.
23. Ardi VC, Van den Steen PE, Opdenakker G, Schweighofer B, Deryugina EI, Quigley JP. Neutrophil MMP-9 proenzyme, unencumbered by TIMP-1, undergoes efficient activation in vivo and catalytically induces angiogenesis via a basic fibroblast growth factor (FGF-2)/FGFR-2 pathway. *J Biol Chem.* 2009;284(38):25854-25866.
24. Murakami M, Simons M. Fibroblast growth factor regulation of neovascularization. *Curr Opin Hematol.* 2008;15(3):215-220.
25. Gregory AD, Capoccia BJ, Woloszynek JR, Link DC. Systemic levels of G-CSF and interleukin-6 determine the angiogenic potential of bone marrow resident monocytes. *J Leukoc Biol.* 2010;88(1):123-131.
26. Magnusson PU, Dimberg A, Mellberg S, Lukinius A, Claesson-Welsh L. FGFR-1 regulates angiogenesis through cytokines interleukin-4 and pleiotrophin. *Blood.* 2007;110(13):4214-4222.
27. Jin DK, Shido K, Kopp HG, et al. Cytokine-mediated deployment of SDF-1 induces revascularization through recruitment of CXCR4+ hemangiocytes. *Nat Med.* 2006;12(5):557-567.
28. Heissig B, Werb Z, Rafii S, Hattori K. Role of c-kit/Kit ligand signaling in regulating vasculogenesis. *Thromb Haemost.* 2003;90(4):570-576.
29. Heissig B, Rafii S, Akiyama H, et al. Low-dose irradiation promotes tissue revascularization through VEGF release from mast cells and MMP-9-mediated progenitor cell mobilization. *J Exp Med.* 2005;202(6):739-750.
30. Heissig B, Lund LR, Akiyama H, et al. The plasminogen fibrinolytic pathway is required for hematopoietic regeneration. *Cell Stem Cell.* 2007; 1(6):658-670.
31. Renckens R, Roelofs JJTH, De Waard V, et al. The role of plasminogen activator inhibitor type 1 in the inflammatory response to local tissue injury. *J Thromb Haemost.* 2005;3(5):1018-1025.
32. Park K-W, Kwon Y-W, Cho H-J, et al. G-CSF exerts dual effects on endothelial cells–Opposing actions of direct eNOS induction versus indirect CRP elevation. *J Mol Cell Cardiol.* 2008;45(5): 670-678.
33. Kanellakis P, Slater NJ, Du XJ, Bobik A, Curtis DJ. Granulocyte colony-stimulating factor and stem cell factor improve endogenous repair after myocardial infarction. *Cardiovasc Res.* 2006;70(1):117-125.
34. Minnerup J, Heidrich J, Wellmann J, Rogalewski A, Schneider A, Schabitz WR. Meta-analysis of the efficacy of granulocyte-colony stimulating factor in animal models of focal cerebral ischemia. *Stroke.* 2008; 39(6):1855-1861.
35. Muhs BE, Gagne P, Plitas G, Shaw JP, Shamamian P. Experimental hindlimb ischemia leads to neutrophil-mediated increases in gastrocnemius MMP-2 and -9 activity: a potential mechanism for ischemia induced MMP activation. *J Surg Res.* 2004;117(2):249-254.
36. May AE, Kanse SM, Lund LR, Gisler RH, Imhof BA, Preissner KT. Urokinase receptor (CD87) regulates leukocyte recruitment via beta 2 integrins in vivo. *J Exp Med.* 1998;188(6):1029-1037.
37. Zhao Y, Sharma AK, LaPar DJ, et al. Depletion of tissue plasminogen activator attenuates lung ischemia-reperfusion injury via inhibition of neutrophil extravasation. *Am J Physiol Lung Cell Mol Physiol.* 2011;300(5):L718-L729.
38. Reichel CA, Lerchenberger M, Uhl B, et al. Plasmin inhibitors prevent leukocyte accumulation and remodeling events in the postischemic microvasculature. *PLoS One.* 2011;6(2):e17229.

STEM CELLS AND DEVELOPMENT
Volume 21, Number 16, 2012

DOI: 10.1089/scd.2012.0065

Identification of Rat *Rosa26* Locus Enables Generation of Knock-In Rat Lines Ubiquitously Expressing *tdTomato*

Toshihiro Kobayashi,[1,2] Megumi Kato-Itoh,[1,2] Tomoyuki Yamaguchi,[1,2] Chihiro Tamura,[2,3] Makoto Sanbo,[3,4] Masumi Hirabayashi,[3,4] and Hiromitsu Nakauchi[1,2]

Recent discovery of a method for derivation and culture of germline-competent rat pluripotent stem cells (PSCs) enables generation of transgenic rats or knock-out rats via genetic modification of such PSCs. This opens the way to use rats, as is routine in mice, for analyses of gene functions or physiological features. In mouse or human, one widely used technique to express a gene of interest stably and ubiquitously is to insert that gene into the *Rosa26* locus via gene targeting of PSCs. *Rosa26* knock-in mice conditionally expressing a reporter or a toxin gene have contributed to tracing or ablation of specific cell lineages. We successfully identified a rat orthologue of the mouse *Rosa26* locus. Insertion of *tdTomato*, a variant of red fluorescent protein, into the *Rosa26* locus of PSCs of various rat strains allows ubiquitous expression of *tdTomato*. Through germline transmission of one *Rosa26-tdTomato* knock-in embryonic stem cell line, we also obtained *tdTomato* knock-in rats. These expressed *tdTomato* ubiquitously throughout their bodies, which indicates that the rat *Rosa26* locus conserves functions of its orthologues in mouse and human. The new tools described here (targeting vectors, knock-in PSCs, and rats) should be useful for a variety of research using rats.

Introduction

USE OF RATS FOR STUDIES in behavior, pharmacology, and disease modeling has been limited because gene-targeting technology has been lacking. However, recent discovery of a culture system using small molecules specifically to inhibit spontaneous differentiation pathways of pluripotent stem cells (PSCs) [1] has permitted generation of germline-competent rat PSCs [2–4]. This stable and reproducible culture system in rat PSCs constitutes a breakthrough for generating not only transgenic rats by introducing exogenous genes into PSCs [5,6], but also knock-out rats via gene targeting [7]. Various genetically modified rats will soon be available for analyses of gene functions or physiological features like those that can now be done in mice.

To generate a genetically modified animal with stable and ubiquitous expression of a gene of interest is essential for current research. One widely used method is to insert that gene into the *Rosa26* locus on mouse chromosome 6, identified by random retroviral gene-trap screening using mouse embryonic stem cells (ESCs) [8]. *Rosa26* is ubiquitously expressed in embryonic as well as adult tissue, and gene targeting at this locus in ES cells is highly efficient. Insertion of a gene of interest or a *loxP*-flanked stop codon with a reporter or a toxin gene into *Rosa26* thus has been widely used to trace specific cell lineages or, by mating with mice expressing *Cre* recombinase under the control of specific promoters, to ablate specific cell lineages [9,10].

As in the mouse, so in man: A human *ROSA26* locus has also been identified by homology search with mouse *Rosa26* sequences [11]. Insertion of sequences encoding a red fluorescent protein (RFP) into the *Rosa26* locus of human ESCs allows ubiquitous expression of *RFP* in both undifferentiated and differentiated states [11]. Features of the *Rosa26* locus may be conserved in a variety of species.

Here, as a third model, we report identification of a *Rosa26* locus in the rat. Furthermore, we generated rat PSCs expressing *tdTomato*, a variant of *RFP*, by gene targeting into the *Rosa26* locus, and generated a knock-in rat line via germline transmission of such PSCs.

Materials and Methods

Animals

C57BL/6NCrSlc, BDF1, and ICR mice and Wistar and DA rats were purchased from SLC Japan (Shizuoka, Japan). All experiments were performed in accordance with the animal

[1]Division of Stem Cell Therapy, Center for Stem Cell Biology and Regenerative Medicine, Institute of Medical Science, University of Tokyo, Tokyo, Japan.
[2]Japan Science Technology Agency, ERATO, Nakauchi Stem Cell and Organ Regeneration Project, Tokyo, Japan.
[3]Center for Genetic Analysis of Behavior, National Institute for Physiological Sciences, Okazaki, Aichi, Japan.
[4]School of Life Science, The Graduate University for Advanced Studies, Okazaki, Aichi, Japan.

care and use committee guidelines of the Institute of Medical Science, the University of Tokyo, and of the National Institute for Physiological Sciences.

Culture of PSCs

In this study, 3 ESC lines and 2 induced PSC (iPSC) lines were used (see Table 1). Their culture conditions were as described [12]. In brief, undifferentiated rat PSCs were maintained on mitomycin-C - treated mouse embryonic fibroblasts in an N2B27 medium [1] containing 1 μM PD0325901 (Axon, Groeningen, The Netherlands), 3 μM CHIR99021 (Axon), and 1,000 U/mL of rat leukemia inhibitory factor (Millipore, Bedford, MA).

DA rat-derived ESC (DA3i-1) and iPSC (DAT3-1) lines were newly established. DA3i-1 ESCs were derived from DA rat blastocysts as described [13]. DAT3-1 iPSC were generated from DA rat-derived tail-tip fibroblasts by introducing 3 mouse factors (*Oct3/4*, *Klf4*, and *Sox2*) in one retroviral vector (data not shown).

Construction of vectors and gene targeting

Homology arms were amplified from genomic DNA of DA strain rats by polymerase chain reaction (PCR) using PrimeSTAR or PrimeSTAR GXL DNA polymerase (Takara Bio, Otsu, Japan), according to the manufacturer's protocol. These arms, with an additional *Nhe*I site and an MC1-promoter driven DTA cassette amplified from an MC1-DTA vector, a kind gift from Dr. T. Yagi (Osaka University, Osaka, Japan), were inserted into pBluescript KS(+) (Stratagene, La Jolla, CA) with an infusion cloning kit (Takara Bio) (*prRosa26-1* in Fig. 1A). A splice acceptor sequence amplified from a *pSAβ-geo* vector, a kind gift from Dr. P. Soriano (Fred Hutchinson Cancer Research Center, Seattle, WA); *tdTomato* amplified from *ptdTomatoN1* (Clontech, Palo Alto, CA); and *IRES-Puro^r-pA* amplified from *pCAG-Cre-IRES-Puro^r-pA*, a kind gift from Dr. J. Miyazaki (Osaka University), were inserted into the *Nhe*I site of *prRosa26-1*.

Electroporation for gene targeting was carried out as described [5]. In brief, $2.5 \sim 5 \times 10^6$ rat PSCs suspended in PBS were mixed with 20 μg linearized targeting vector digested by the *Sal*1 restriction enzyme and were transferred to a Gene Pulser cuvette (Bio-Rad, Richmond, CA). Electroporation was carried out at 800 V, 10 μF in Gene Pulser equipment (Bio-Rad). After electroporation, PSCs were seeded onto mitomycin-C - treated puromycin-resistant mouse embryonic fibroblasts made in house, and 24 h later, 1.5 μg/mL puromycin (Invitrogen, Carlsbad, CA) was added to the culture medium.

Reverse transcription–PCR and quantitative real-time PCR analysis

cDNA synthesized using the ThermoScript™ reverse transcription (RT)–PCR System (Invitrogen, Carlsbad, CA) from extracts of BLK2i-1 rat ESCs was used for the RT-PCR analysis of *Rosa26* noncoding RNA. PCR primers are shown in Supplementary Fig. S3 (Supplementary Data are available online at www.liebertpub.com/scd). One forward primer and 4 reverse primers were designed (F1 and R1-R4, shown in Fig. 1A and Supplementary Fig. S3). PCR was performed using Taq HS polymerase (Takara Bio) according to the manufacturer's protocol.

3′ and 5′ rapid amplification of cDNA ends analysis and identification of full-length noncoding RNA

3′ and 5′ rapid amplification of cDNA ends (RACE) was performed using the SMARTer™ RACE cDNA Amplification Kit (Clontech), according to the manufacturer's protocol. Synthesized cDNAs were amplified using an universal primer A mix with 3′ or 5′ RACE primers (primers shown in Supplementary Fig. S3). Amplified cDNAs were cloned into the pCR-Blunt IITOPO vector (Invitrogen), and their sequences were confirmed.

Genotyping and Southern blotting

DNA was extracted using QIAamp DNA Mini Kits (Qiagen, Germantown, MD) from picked-up PSCs. For genotyping, PCR primers for amplification of the *Rosa26* knock-in locus were Fw, 5′-CAGAAAAGGCGGAGCGAGCCCAAG-3′, and Rv, 5′- GGGCCCTCACATTGCCAAAAGACGG-3′. For the Southern blot analysis, genomic DNA extracted from PSCs was digested by the *Apa*I restriction enzyme and hybridized with a DNA probe cloned from the upstream region of the rat *Rosa26* 5′-arm.

Embryo manipulation

Rat and mouse embryos were prepared using published protocols [12,14]. In brief, rat blastocysts were collected in the

TABLE 1. EFFICIENCY OF GENE TARGETING IN VARIOUS TYPES OF RAT PLURIPOTENT STEM CELLS

Name	*Strain*	*Cell type*	*Reference*	*Transduced cells*	*Drug- resistant colonies*	*Picked- up colonies*	*Targeted clones (%)*[a]
BLK2i-1	DA×Wistar	ESC	[18]	5×10e6	3	2	1 (50)
				5×10e6	2	2	2 (100)
				2.5×10e6	18	12	6 (50)
DA3i-1	DA	ESC		5×10e6	48	24	9 (38)
BN2i-4	BN	ESC	[5]	5×10e6	8	8	2 (25)
				5×10e6	13	9	2 (23)
T1-3	Wistar	iPSC	[4,12]	4×10e6	9	8	3 (38)
DAT3-1	DA	iPSC		5×10e6	6	6	1 (17)
Total					107	71	26 (37)

[a]Judged by PCR.
ESC, embryonic stem cell; iPSC, induced pluripotent stem cell; PCR, polymerase chain reaction.

HER medium [15] containing 18% fetal bovine serum (Invitrogen) from the oviduct and the uterus of rats 4.5 days post coitum (dpc). These embryos were transferred into the mR1ECM medium [16] containing 80 mM NaCl and 0.01% polyvinyl alcohol (Sigma-Aldrich Co., St. Louis, MO) and were cultured for about 1 h until injection. Mouse 8-cell/morula stage embryos were collected in the M2 medium (Millipore) from the oviduct and the uterus of BDF1 × C57BL/6 mice 2.5 dpc. These embryos were transferred into the KSOM-AA medium (Millipore) and were cultured for 24 h before blastocyst injection.

For micromanipulation, PSCs were trypsinized and suspended in the PSC culture medium. A piezo-driven micromanipulator (Prime Tech, Tokyo, Japan) was used to drill zona pellucida and trophectoderm under the microscope, and 10 PSCs were introduced into blastocyst cavities near the inner cell mass. After blastocyst injection, embryos underwent follow-up culture for 1–2 h. Rat blastocysts were transferred into the uteri of pseudopregnant recipient Wistar rats (3.5 dpc), and mouse blastocysts were transferred into the uteri of pseudopregnant recipient ICR mice (2.5 dpc).

Flow cytometry analysis

To analyze chimerism of chimeric rats at the adult stage, we used peripheral blood cells obtained from the retro-orbital venous plexus. Leukocytes isolated by osmotic lysis of erythrocytes were stained with APC-conjugated mouse anti-rat CD45 antibody (BD Biosciences, San Diego, CA).

To analyze chimerism of interspecific chimeras at the fetal stage, embryonic fibroblasts were stained with biotin-conjugated mouse anti-rat CD54 antibody (ICAM-1, 1A29), Alexa Fluor 647-conjugated goat anti-mouse IgG antibody, and FITC-conjugated rat anti-mouse CD54 antibody (all BD Biosciences).

All stained cells were analyzed by FACSCanto II (BD Bioscience).

Result and Discussion

Given that the transgenic rat carrying a mouse *Rosa26* promoter-driven *EGFP* construct revealed ubiquitous expression of *EGFP* [17], we inferred that the promoter region

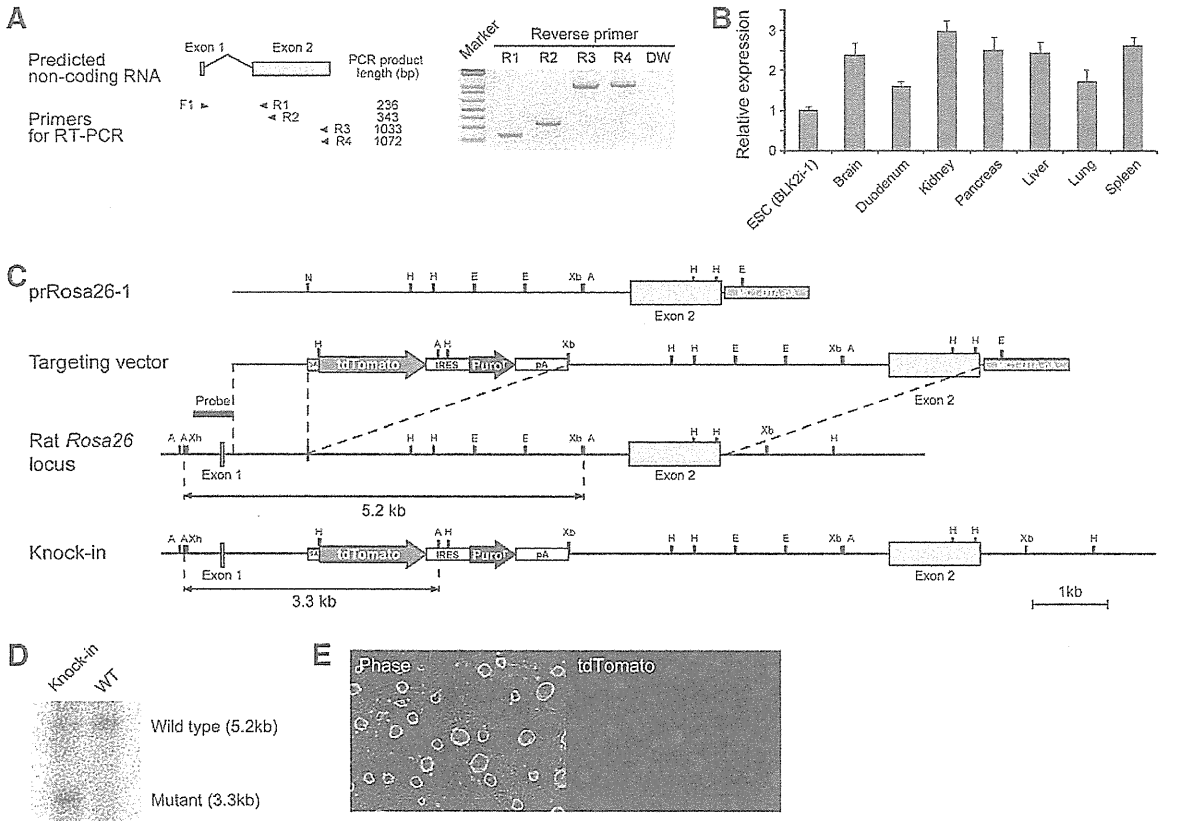

FIG. 1. Identification of Rat *Rosa26* locus and gene targeting of rat pluripotent stem cells by inserting a cassette containing *tdTomato* into *Rosa26* locus. **(A)** The RT-PCR analysis of rat *Rosa26* noncoding RNA in rat ESCs. The primer positions are schematically shown by *arrowheads* under the predicted noncoding RNA transcript. **(B)** Quantitative real-time PCR of *Rosa26* noncoding RNA in rat ESCs and adult tissues relative to *β-actin*. Error bars are mean ± SD ($n = 2$). **(C)** Structure of targeting vectors and a schematic of knock-in genome of rat *Rosa26* locus on chromosome 4. Letters on the locus indicate selected restriction enzyme sites. A, *Apa*I; E, *Eco*R1; H, *Hin*dIII; N, *Nhe*I; Xb, *Xba*I; Xh, *Xho*I. **(D)** Result of the Southern blot analysis using ApaI-digested genomic DNA hybridized with 5′ probe schematically shown in **(A)**. **(E)** Photomicrograph of *Rosa26-tdTomato* knock-in rat ESCs generated from the BLK2i-1 line (BLK-RT2). These ESCs express *tdTomato* ubiquitously. ESCs, embryonic stem cells; RT-PCR, reverse transcription–polymerase chain reaction.

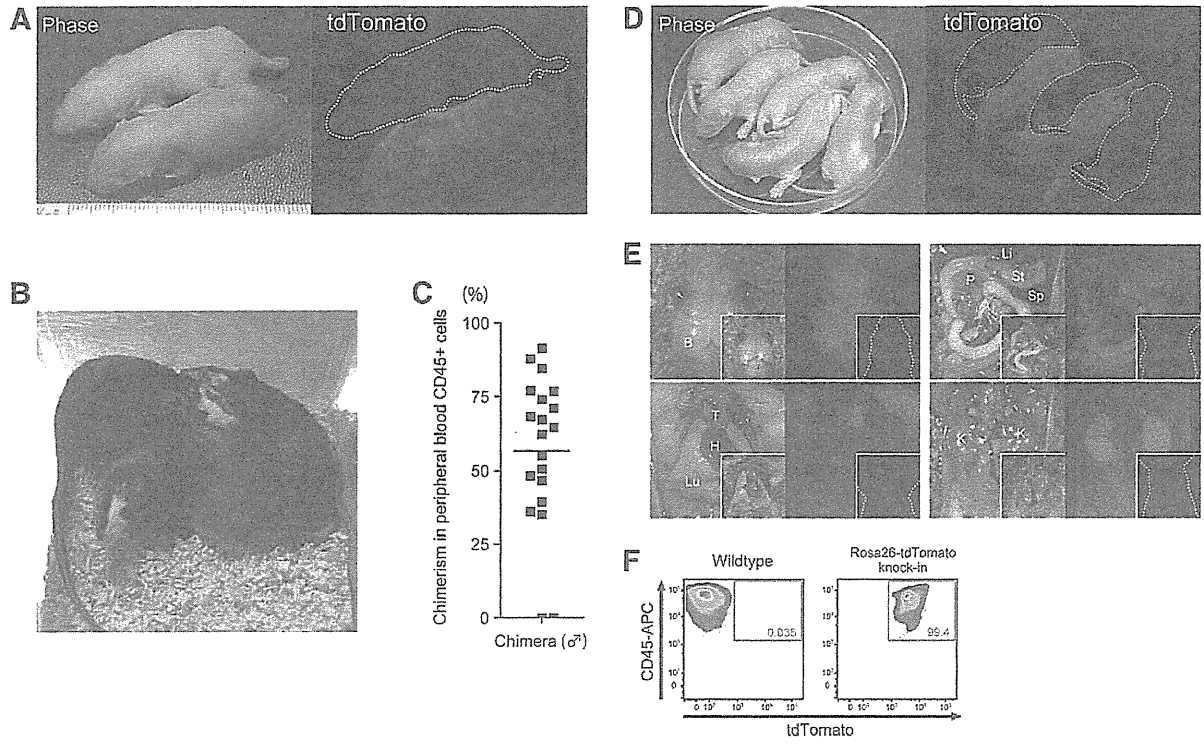

FIG. 2. Generation of chimeric rats by injection of *Rosa26-tdTomato* knock-in rat ESCs into rat blastocysts. **(A)** Picture of a representative newborn chimeric rat generated by intrablastocystic injection of BLK-RT2 rat ESCs. Rat not expressing *tdTomato* is a nonchimeric littermate (*white dashed outline*). **(B)** Adult chimeric rats. Black coat color originates from injected ESCs; white coat color originates from host blastocysts. **(C)** The chimerism analysis in peripheral blood of male chimeric rats. Leukocytes isolated by osmotic lysis of erythrocytes were stained with antibody against rat CD45 and were analyzed by flow cytometry for intensity of *tdTomato* expression in CD45-positive cells. *Square dots* indicate values for individual rats. **(D)** Offspring obtained by mating a male chimeric rat with a wild-type female. *tdTomato*-positive neonates are *Rosa26-tdTomato* knock-in rats that resulted from germline transmission of genes contained in BLK-RT2 rat ESCs. **(E)** *tdTomato* expression in main organs of *Rosa26-tdTomato* knock-in rats. *Insets* show organs obtained from *tdTomato*-negative littermates (*white-dashed* outline). In *bright-field panels*, B, brain; T, thymus; H, heart; Lu, lung; Li, liver; P, pancreas; St, stomach; Sp, spleen; and K, kidney. **(F)** FACS patterns obtained using peripheral blood cells from wild-type rats and *Rosa26-tdTomato* knock-in rats. In knock-in rats, almost all CD45-positive cells express *tdTomato*. FACS, fluorescence activated cell sorting.

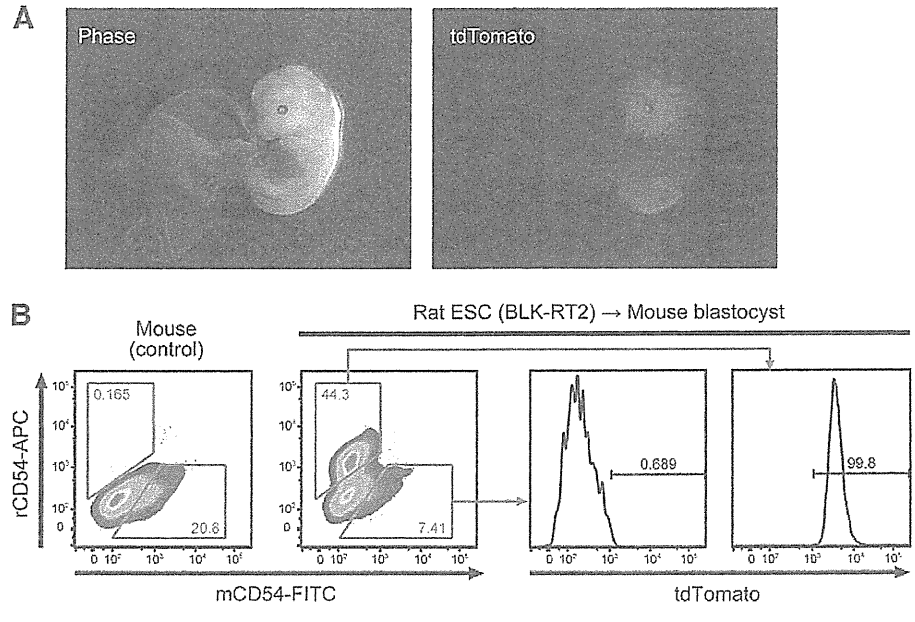

FIG. 3. Generation of interspecific chimeras by injection of *Rosa26-tdTomato* knock-in rat ESCs into mouse blastocysts. **(A)** Embryonic day (E) 13.5 interspecific chimera generated by injection of BLK-RT2 rat ESCs into a mouse blastocyst. **(B)** FACS patterns obtained using embryonic fibroblasts established from an interspecific chimera and stained with a specific antibody against mouse or rat CD54. As a control, mouse embryonic fibroblasts were also analyzed.

of the *Rosa26* locus contained a highly conserved sequence. To identify a *Rosa26* locus in rat genome, we searched for similar sequences in the UCSC Genome Browser database (http://genome.ucsc.edu/) with a 5′ arm 1,088 bp sequence of the mouse *Rosa26* targeting-vector [10], which corresponds to the first intron of the mouse *Rosa26* transcript. We found a highly conserved region in rat chromosome 4 that contains not only a *Rosa26* locus, but also genes that are neighbors to *Rosa26* in mouse (Supplementary Fig. S1). In mice, transcripts from the *Rosa26* locus are ubiquitously expressed noncoding RNAs [8]. To see whether the putative rat *Rosa26* locus also encodes such noncoding RNAs, we confirmed the expression of *Rosa26* in rat ESCs by RT-PCR. We designed primer sets to flank a region containing the first intron, with sequences based on the rat-expressed sequence tag database (Fig. 1A, Supplementary Figs. S2 and S3). Our results showed that 2 exons flanking 1 intron were amplified with each primer set (Fig. 1A and Supplementary Fig. S2). The quantitative real-time PCR analysis demonstrated that this noncoding RNA was expressed in a wide variety of adult tissues (Fig. 1B). To reveal the full-length sequence of this noncoding RNA, we performed the 3′ and 5′ RACE analysis. The sequence of at least one noncoding RNA transcribed from the rat *Rosa26* locus was 1,160 bp long (Supplementary Fig. S2). It exhibited 74% homology with the sequence of one of the mouse *Rosa26* noncoding RNA transcripts (NR_027009) (Supplementary Fig. S3).

To see if this region, like the *Rosa26/ROSA26* locus in mouse or human, actually allowed ubiquitous expression of an inserted gene, we cloned homology arms from genomic DNA of the DA rat and constructed a targeting vector to insert a splice acceptor with the *tdTomato-IRES-Puro^r-pA* sequence (Fig. 1C). We transduced the linearized targeting vector into 3 ESC lines and 2 iPSC lines derived from various strains and tissues. Although only small numbers of colonies were observed after electroporation and drug selection, on average about 30% of picked-up clones demonstrated correct targeting judged by PCR using genomic DNA (Table 1). Gene targeting was also confirmed by Southern blotting (Fig. 1D). As expected, all positive clones ubiquitously expressed *tdTomato* (Fig. 1E). Survival rates of PSCs after drug selection were low compared with mouse PSCs subjected to conventional targeting. This might result from low transduction efficiency of the targeting vector or from high sensitivity to antibiotics in rat PSCs [7].

We injected rat ESCs from one of the *Rosa26-tdTomato* knock-in lines, BLK-RT2, into rat blastocysts. Rat ESCs of the original cell line, BLK2i-1, are germline-competent. The line was established from blastocysts of rats with black coats derived from F1 crosses of Wistar (white-coated) and DA (black-coated) rats back-crossed with Wistar rats for at least 3 generations [18]. A total of 116 injected blastocysts were transferred into uteri of pseudo-pregnant rats and at weaning 27 out of 36 pups proved chimeras. Neonatal chimeric rats expressed *tdTomato* throughout their bodies (Fig. 2A). They grew into adults normally and showed coat color chimerism (black, donor ESC-derived; white, host embryo Wistar strain-derived) (Fig. 2B). To estimate their chimerism, we analyzed *tdTomato* expression in peripheral blood of male chimeric rats by flow cytometry. Although chimerism varied individually, most chimeras showed over 50% chimerism in CD45-positive peripheral blood mononuclear cells (Fig. 2C).

Next, we mated 3 male rats exhibiting relatively higher chimerism with wild-type females to see if BLK-RT2 rat ESCs were capable of germline transmission. Offspring of 2 chimeras expressed *tdTomato* ubiquitously throughout their bodies, indicating successful germline transmission (Fig. 2D). Expression of *tdTomato* was detected in all main organs at the neonatal stage (Fig. 2E) and in CD45-positive blood cells at the adult stage (Fig. 2F). These data provided strong evidence for functional conservation of the *Rosa26/ROSA26* locus among rat, mouse, and human.

We also injected BLK-RT2 rat ESCs into mouse blastocysts. A total of 32 injected blastocysts were transferred into uteri of pseudo-pregnant mice, and 13 out of 16 fetuses proved interspecific chimeras (Fig. 3A). To distinguish host- and donor-derived cells, we cultured embryonic fibroblasts from these chimeras and stained them with a specific antibody against mouse or rat CD54. Only cells expressing rat CD54 also expressed *tdTomato* (Fig. 3B). Therefore, *Rosa26* knock-in rat PSCs can also be used for interspecific blastocyst complementation to make rat organs in mice [12].

Via gene targeting of PSCs, we have successfully generated *Rosa26* knock-in rats that express *tdTomato* ubiquitously. These PSCs and rats will provide useful tools for cellular or organ transplantation experiments, and the targeting vector constructed here will be useful for expressing genes of interest stably and ubiquitously in a variety of rat PSCs. These powerful tools should contribute to progress in a variety of research using rats.

Acknowledgment

We thank Dr. A. Knisely for critical reading of the article. This work was supported by grants from the Japan Science and Technology Agency (JST), KAKENHI (23700507) Grant-in-Aid for Young Scientists (B) from Japan Society for the Promotion of Science (JSPS), and the Ministry of Education, Culture, Sport, Science, and Technology (MEXT).

Author Disclosure Statement

Hiromitsu Nakauchi is a founder and shareholder of ReproCELL, Inc. There is no conflict of interest to disclose.

Reference

1. Ying QL, J Wray, J Nichols, L Batlle-Morera, B Doble, J Woodgett, P Cohen and A Smith. (2008). The ground state of embryonic stem cell self-renewal. Nature 453:519–523.
2. Buehr M, S Meek, K Blair, J Yang, J Ure, J Silva, R McLay, J Hall, QL Ying and A Smith. (2008). Capture of authentic embryonic stem cells from rat blastocysts. Cell 135:1287–1298.
3. Li P, C Tong, R Mehrian-Shai, L Jia, N Wu, Y Yan, RE Maxson, EN Schulze, H Song, et al. (2008). Germline competent embryonic stem cells derived from rat blastocysts. Cell 135:1299–1310.
4. Hamanaka S, T Yamaguchi, T Kobayashi, M Kato-Itoh, S Yamazaki, H Sato, A Umino, Y Wakiyama, M Arai, et al. (2011). Generation of germline-competent rat induced pluripotent stem cells. PLoS One 6:e22008.
5. Hirabayashi M, M Kato, M Sanbo, T Kobayashi, S Hochi and H Nakauchi. (2010). Rat transgenesis via embryonic stem cells electroporated with the Kusabira-orange gene. Mol Reprod Dev 77:474.

6. Kawamata M and T Ochiya. (2010). Generation of genetically modified rats from embryonic stem cells. Proc Natl Acad Sci U S A 107:14223–14228.
7. Tong C, P Li, NL Wu, Y Yan and QL Ying. (2010). Production of p53 gene knockout rats by homologous recombination in embryonic stem cells. Nature 467:211–213.
8. Zambrowicz BP, A Imamoto, S Fiering, LA Herzenberg, WG Kerr and P Soriano. (1997). Disruption of overlapping transcripts in the ROSA beta geo 26 gene trap strain leads to widespread expression of beta-galactosidase in mouse embryos and hematopoietic cells. Proc Natl Acad Sci U S A 94:3789–3794.
9. Mao X, Y Fujiwara, A Chapdelaine, H Yang and SH Orkin. (2001). Activation of EGFP expression by Cre-mediated excision in a new ROSA26 reporter mouse strain. Blood 97:324–326.
10. Soriano P. (1999). Generalized lacZ expression with the ROSA26 Cre reporter strain. Nat Genet 21:70–71.
11. Irion S, H Luche, P Gadue, HJ Fehling, M Kennedy and G Keller. (2007). Identification and targeting of the ROSA26 locus in human embryonic stem cells. Nat Biotechnol 25: 1477–1482.
12. Kobayashi T, T Yamaguchi, S Hamanaka, M Kato-Itoh, Y Yamazaki, M Ibata, H Sato, YS Lee, J Usui, et al. (2010). Generation of rat pancreas in mouse by interspecific blastocyst injection of pluripotent stem cells. Cell 142:787–799.
13. Hirabayashi M, M Kato, T Kobayashi, M Sanbo, T Yagi, S Hochi and H Nakauchi. (2010). Establishment of rat embryonic stem cell lines that can participate in germline chimerae at high efficiency. Mol Reprod Dev 77:94.
14. Nagy A, M Gertsenstein, K Vintersten and R Behringer. (2003). *Manipulating the Mouse Embryo A Laboratory Manual*, 3rd edn. Cold Spring Harbor Laboratory Press, Cold Spring Harbor, New York.
15. Ogawa S, K Sato and H Hashimoto. (1971). In vitro culture of rabbit ova from the single cell to the blastocyst stage. Nature 233:422–424.
16. Miyoshi K, LR Abeydeera, K Okuda and K Niwa. (1995). Effects of osmolarity and amino acids in a chemically defined medium on development of rat one-cell embryos. J Reprod Fertil 103:27–32.
17. Kisseberth WC, NT Brettingen, JK Lohse and EP Sandgren. (1999). Ubiquitous expression of marker transgenes in mice and rats. Dev Biol 214:128–138.
18. Hirabayashi M, C Tamura, M Sanbo, T Goto, M Kato-Itoh, T Kobayashi, H Nakauchi and S Hochi. (2012). Ability of tetraploid rat blastocysts to support fetal development after complementation with embryonic stem cells. Mol Reprod Dev79:402–412.

Address correspondence to:
Dr. Hiromitsu Nakauchi
Division of Stem Cell Therapy
Center for Stem Cell Biology and Regenerative Medicine
Institute of Medical Science
University of Tokyo
4-6-1 Shirokanedai
Minato-ku
Tokyo 108-8639
Japan

E-mail: nakauchi@ims.u-tokyo.ac.jp

Received for publication February 9, 2012
Accepted after revision May 7, 2012
Prepublished on Liebert Instant Online May 7, 2012

blood

2012 119: 5405-5416
Prepublished online April 27, 2012;
doi:10.1182/blood-2011-11-390849

MT1-MMP plays a critical role in hematopoiesis by regulating HIF-mediated chemokine/cytokine gene transcription within niche cells

Chiemi Nishida, Kaori Kusubata, Yoshihiko Tashiro, Ismael Gritli, Aki Sato, Makiko Ohki-Koizumi, Yohei Morita, Makoto Nagano, Takeharu Sakamoto, Naohiko Koshikawa, Takahiro Kuchimaru, Shinae Kizaka-Kondoh, Motoharu Seiki, Hiromitsu Nakauchi, Beate Heissig and Koichi Hattori

Blood (print ISSN 0006-4971, online ISSN 1528-0020), is published weekly by the American Society of Hematology, 2021 L St, NW, Suite 900, Washington DC 20036.

MT1-MMP plays a critical role in hematopoiesis by regulating HIF-mediated chemokine/cytokine gene transcription within niche cells

Chiemi Nishida,[1] Kaori Kusubata,[2] Yoshihiko Tashiro,[1] Ismael Gritli,[1] Aki Sato,[1] Makiko Ohki-Koizumi,[1] Yohei Morita,[1] Makoto Nagano,[3] Takeharu Sakamoto,[3] Naohiko Koshikawa,[3] Takahiro Kuchimaru,[4] Shinae Kizaka-Kondoh,[4] Motoharu Seiki,[3] Hiromitsu Nakauchi,[1] *Beate Heissig,[1,2,5] and *Koichi Hattori[1,5]

[1]Center for Stem Cell Biology and Regenerative Medicine, Institute of Medical Science, University of Tokyo, Tokyo, Japan; [2]Frontier Research Initiative, Institute of Medical Science, University of Tokyo, Tokyo, Japan; [3]Division of Cancer Cell Research, Institute of Medical Science, University of Tokyo, Tokyo, Japan; [4]Department of Biomolecular Engineering, Tokyo Institute of Technology, Yokohama, Japan; and [5]Atopy (Allergy) Research Center, Juntendo University School of Medicine, Tokyo, Japan

HSC fate decisions are regulated by cell-intrinsic and cell-extrinsic cues. The latter cues are derived from the BM niche. Membrane-type 1 matrix metalloproteinase (MT1-MMP), which is best known for its proteolytic role in pericellular matrix remodeling, is highly expressed in HSCs and stromal/niche cells. We found that, in MT1-MMP$^{-/-}$ mice, in addition to a stem cell defect, the transcription and release of kit ligand (KitL), stromal cell–derived factor-1 (SDF-1/CXCL12), erythropoietin (Epo), and IL-7 was impaired, resulting in a trilineage hematopoietic differentiation block, while addition of exogenous KitL and SDF-1 restored hematopoiesis. Further mechanistic studies revealed that MT1-MMP activates the hypoxia-inducible factor-1 (HIF-1) pathway via factor inhibiting HIF-1 (FIH-1) within niche cells, thereby inducing the transcription of HIF-responsive genes, which induce terminal hematopoietic differentiation. Thus, MT1-MMP in niche cells regulates postnatal hematopoiesis, by modulating hematopoietic HIF-dependent niche factors that are critical for terminal differentiation and migration. (*Blood*. 2012;119(23):5405-5416)

Introduction

The adult hematopoietic system is maintained by a small number of HSCs that reside in the BM in a specialized microenvironment (the niche).[1,2] Here, HSCs undertake fate decisions including differentiation to progenitor cells and self-renewal, which ensures a lifelong supply of terminally differentiated blood cells. Intrinsic cellular programming and external stimuli such as adhesive interactions with the microenvironmental stroma and cytokine activities regulate HSC fate. However, it is unclear how niche factor production is controlled to adjust to external demand with a fine-tuned response.

Hypoxia-inducible factors (HIFs) consist of an α (HIF-α) and a β (HIF-β, or ARNT) subunit and activate the expression of genes encoding proteins that regulate cell metabolism, motility, angiogenesis, hematopoiesis, and other functions. HSCs maintain cell-cycle quiescence by regulating HIF-1α levels.[3,4] Mice with mutations in the heterodimeric transcription factor HIF develop extensive hematopoietic pathologies: embryos lacking *Arnt* have defects in primitive hematopoiesis.[5] Mice lacking endothelial PAS domain protein 1 (EPAS1, also known as HIF-2alpha/HRF/HLF/MOP3), a second HIF family member, exhibited pancytopenia, and it was shown that EPAS1 is necessary to maintain a functional microenvironment in the BM for effective hematopoiesis.[6] HIFs bind to canonical DNA sequences in the promoters or enhancers of target genes such as erythropoietin (*Epo*), vascular endothelial growth factor-A, *SDF-1*α/CXCL12, angiopoietin-2, platelet-derived growth factor-B and Kit Ligand (*KitL*)/stem cell factor, which are involved in HSC maintenance within the BM niche.[7-10] The chemokine SDF-1α/CXCL12 (SDF-1α) is expressed by perivascular, endosteal, mesenchymal stem and progenitor cells as well as by osteoblasts.[11,12] SDF-1α deficiency leads to a reduction in HSCs and impaired B-cell development in mice.[13,14] IL-7 is another stromal cell–derived niche factor, which, in cooperation with CXCL12, functions at sequential stages of B-cell development.[15,16] IL-7 or IL-7R deficiency results in impaired B-cell development.[17,18]

Proteases such as matrix metalloproteinase-9 (MMP-9) and the serine proteinase plasmin(ogen) regulate HSC fate through KitL release in the BM.[10,19] Membrane type-1 MMP (MT1-MMP, also known as MMP-14) can proteolytically degrade extracellular matrix (ECM) components and cleave membrane receptors and ligands.[20] MT1-MMP is expressed within mesenchymal stem and immature hematopoietic cells.[21,22] MT1-MMP can control the migration of hematopoietic stem/progenitor cells and monocytes.[21,23,24] MT1-MMP function is essential for angiogenesis, wound healing, connective tissue remodeling, arthritis, tumor growth, and metastasis.[25-27] MT1-MMP–deficient (MT1-MMP$^{-/-}$) mice showed skeletal dysplasia, arthritis, and osteopenia.[28] However, the role of MT1-MMP in hematopoiesis is unclear.

We found that MT1-MMP inactivation in mice resulted in severe pancytopenia, characterized by an impaired stem cell pool and a block in hematopoietic differentiation. MT1-MMP deletion from hematopoietic cells generated normal hematopoiesis in recipient mice, thereby demonstrating that MT1-MMP is an essential regulator of the BM microenvironment. Mechanistically, we demonstrate that MT1-MMP deficiency blocked the transcription of

Submitted November 8, 2011; accepted April 21, 2012. Prepublished online as *Blood* First Edition paper, April 27, 2012; DOI 10.1182/blood-2011-11-390849.

*B.H. and K.H. share senior authorship.

The online version of this article contains a data supplement.

The publication costs of this article were defrayed in part by page charge payment. Therefore, and solely to indicate this fact, this article is hereby marked "advertisement" in accordance with 18 USC section 1734.

typical HIF-1–dependent niche factors including Epo, SDF-1, KitL, and IL-7 by modulating the HIF-1 pathway through factor inhibiting HIF-1 (FIH1), resulting in a 3-lineage terminal differentiation block. Thus, MT1-MMP controls HSC fate by regulating the BM niche.

Methods

Animals

Age-matched (14-day) MT1-MMP$^{+/+}$ and MT1-MMP$^{-/-}$ mice were obtained by heterozygous breeding.[24] Animal procedures were approved by the Animal Care Committee of The Institute of Medical Science (University of Tokyo). C57BL/6 and C57BL/6-Tg (CAG-EGFP) mice were purchased from Japan SLC Inc, and Ly5.1 mice were purchased from Sankyo Lab Service.

In vivo assays

Competitive transplantation experiments. Lethally irradiated Ly-5.1 mice were injected with BM cells (10 recipient mice per cell concentration) from MT1-MMP$^{+/+}$ or MT1-MMP$^{-/-}$ mice together with 2×10^5 CD45.1 BM competitive cells. Peripheral blood (PB) cells of the recipient mice were analyzed 4 months after transplantation. Cells were stained with PE-conjugated anti-CD4 and anti-CD8, FITC-conjugated anti-CD45.2, allophycocyanin-conjugated anti-CD11b and anti-Gr-1, PE-cy7–conjugated anti-B220, and biotinylated anti-CD45.1 Abs. The biotinylated Ab was developed using streptavidin-PE–Cy5. The percentage of donor-derived lineage contributions in PBMCs was assessed using Abs against CD45.2, Gr-1/CD11b, or B220. Total chimerism of > 1% for all Abs tested using PBMCs was considered as long-term reconstitution. The frequencies were determined using L-Calc software (StemCell Technologies).

Growth factor rescue experiments. Recombinant mouse KitL (PeproTech) was administered IP into MT1-MMP$^{+/+}$ and MT1-MMP$^{-/-}$ mice at a concentration of 150 μg/kg body weight, daily from postnatal day 7 to day 10. Recombinant mouse SDF-1α (PeproTech; 100 ng/mice) was injected twice intraperitoneally on postnatal day 10. Blood was collected and blood cells counted on day 12.

CFU-S assay. Mobilized PBMCs were obtained and subjected to a CFU-S assay as previously described.[29] Mice were killed on day 12. The number of visible splenic colonies was counted.

In vitro assays

Peripheral blood analysis. Blood was collected from mice by retro-orbital bleeding using heparinized capillaries. White blood cell (WBC), RBC, and platelet (PLT) counts were determined. Plasma samples were stored at −80°C until further analysis.

Hematopoietic progenitor assay. BM mononuclear cells (BMMCs; 10^4 cells/plate) were plated in triplicate in 1 mL of a commercially available methylcellulose-based assay solution (Methocult; StemCell Technologies).

Lineage-negative cell separation. Murine BM cells were obtained after flushing mouse femur and tibiae. Cells were stained using a lineage cell separation kit (StemCell Technologies). After MACS cell separation (Miltenyi Biotec), cells were stained with c-Kit, Sca-1, and lineage Abs (BD Pharmingen), and were then analyzed by FACS.

B-cell colony-forming assay (CFU–IL-7). The CFU–IL-7 assay was carried out in medium (Invitrogen) containing 1.2% methylcellulose (StemCell Technologies), 30% FCS (HyClone), 1% BSA, 0.1mM 2-ME, and mouse IL-7 (PeproTech). On day 7 of culture, aggregates consisting of > 50 cells were scored as a colony.

Cell culture. Mouse stromal cells (MS-5) were maintained in IMDM supplemented with 10% FBS. Human BM endothelial cells (BMEC-1) were maintained in Medium 199 supplemented with 10% FBS, 0.146 mg/mL L-glutamine, and 2.2 mg/mL sodium bicarbonate. Mouse embryonic fibroblast cells (NIH3T3) were maintained in DMEM supplemented with 10% FBS. These cells were cultured at 37°C, in a 5% CO_2 incubator. Human osteoblastic cells (FOB) were maintained in a 1:1 mixture of Ham F12 medium DMEM supplemented with 2.5mM L-glutamine and 10% FBS, and the cells were cultured at 34°C, in a 5% CO_2 incubator. MT1-MMP$^{+/+}$ and MT1-MMP$^{-/-}$ mouse embryonic fibroblasts (MEF) cells (kindly provided by M.S.) were maintained in DMEM (Invitrogen) supplemented with 10% FBS at 37°C, in a 5% CO_2 incubator.[30]

Knockdown experiment using shRNA. The shRNA sequences used for knockdown of mouse MT1-MMP and FIH-1 were: 5′-caccgctgtggtgttc-cggataagtcgaaacttatccggaacaccacagc-3′ and 5′-caccggacctcgaatacctgcaagac-gaatcttgcaggtattcgaggtccttttt-3′, respectively. These sequences were subcloned into pENTR/U6 TOPO (Invitrogen) and then transferred via recombination into the lentivirus vector pLenti6 BLOCKiT (Invitrogen). shRNA-expressing lentiviral vectors were generated and used according to the manufacturer's instructions.

FACS analysis. Cells were flushed out from mouse BM. For cell-surface analysis, cells were stained with the following Abs: PE-conjugated anti-CD19, -Sca-1, -B220, CD44, c-kit, and -Gr1, FITC-conjugated anti-CD43, -CD34, -NK1.1, and -CD8, allophycocyanin-conjugated anti-B220, -CD4, CD11b, and a lineage cocktail, PerCP-Cy5.1–conjugated anti-c-kit. Cells were analyzed using FACS Aria (BD Biosciences). Common myeloid progenitor (CMP), granulocyte/macrophage progenitor (GMP), and megakaryocyte/erythroid progenitor (MEP) were determined in Lin$^-$ BM cells of 14-day-old MT1-MMP$^{+/+}$ and MT1-MMP$^{-/-}$ mice. The following Abs were used: c-kit–allophycocyanin, Sca1-PE/Cy7, CD34-FITC, FcgRIII-PE all from BD Pharmingen. For the detection of Lin$^-$ cells, biotinylated Abs (B220-bio, Gr-1-bio, CD11b-bio, CD5-bio, Ter119-bio, 7-4-bio, from Miltenyi Biotec) were costained with allophycocyanin/Cy7-conjugated (BD Biosciences/BD Pharmingen) streptavidin. For mesenchymal stem cells (MSCs) detection, cells were stained with the following Abs: CD45-PE, Sca1-FITC, PDGFRα-allophycocyanin (eBioscience), TER119-PE (BD Bioscience), CD45–Pacific Blue (BioLegend), and Alexa 488–conjugated nestin Ab (Abcam).

RNA extraction, RT-PCR, and quantitative real-time PCR analysis. Total RNA was extracted using RNA TRIzol (Invitrogen), and cDNA was generated according to the manufacturer's protocols. This cDNA (10 ng) was used as a template for each PCR amplification using the following specific forward and reverse primers, respectively: mouse *β-actin* (5′-tggaatcctgtggcatccatgaaac-3′) and (5′-taaaacgcagctcagtaacagtccg-3′); mouse *MT1-MMP* (5′-tccggataagtttgggactg-3′) and (5′-ccttcaccatcaaagggtgt-3′); human *GAPDH* (5′-gagtcaacggatttggtcgt-3′) and (5′-ttgattttggagggatctcg-3′); human *MT1-MMP* (5′-caagcattgggtgtttgatgatg-3′) and (5′-cttggggtactcgctatcca-3′). For quantitative real-time PCR, PCR mixtures were prepared using SYBR Premix Ex TaqII (Takara) containing 0.2mM of each primer, and amplification reactions were performed. Specific forward and reverse primers, respectively, were designed as follows: *β-actin* (5′-gctggaaggtggacagtgag-3′) and (5′-tgacaggatgcagaaggaga-3′); *KitL* (5′-gcctagtcattgttggctac-3′) and (5′-cccaagtttgtctatgatgg-3′); *SDF-1* (5′-agaaaccttccaccagagca-3′) and (5′-aacggctaggaaagggtctc-3′); *IL-7* (5′-tgcaatcatgtcaactgcaa-3′) and (5′-tgcaatcatgtcaactgcaa-3′); *EPO* (5′-catctgcgacagtcgagttctg-3′) and (5′-cacaacccatcgtgacattttc-3′); *G-CSF* (5′-cctgcttagagcagagagag-3′) and (5′-cagcagcaggaatcaatact-3′). Gene expression levels were measured using the ABI Prism 7500 sequence detection system (Applied Biosystems). PCR product levels were estimated by measurement of the intensity of SYBR Green fluorescence. Gene expression levels were normalized to *β-actin* mRNA.

Knockdown experiment using siRNA. Target sequences for siRNA were commercially designed and synthesized (B-bridge). siRNAs were provided as a mixture containing 3 different siRNA target sequences. The RNAi transfection solution was prepared by preincubating a mixture of 5nM siRNAs dissolved in 1 mL of serum-free and antibiotic-free medium (OptiMEM; Invitrogen) and 10 μL of RNAiMAX for 20 minutes at room temperature. Cells ($3\text{-}4.5 \times 10^5$ cell/4 mL growth medium without antibiotics) suspended by trypsinization were added to the mixture and cultured overnight, and the medium was replaced with fresh growth medium.

Overexpression of MT1-MMP. The transfection solution was prepared by preincubating a mixture of 1 μg of plasmid DNA dissolved in 250 μL of OptiMEM and 3 μL of Lipofectamine 2000 (Invitrogen) dissolved in 250 μL of OptiMEM for 20 minutes at room temperature. The transfection mixture (500 μL in total) was then added to the cells. After

48 hours of culture, the culture media were replaced with fresh growth medium.

Immunoprecipitation. Cells were lysed with cell lysis buffer (Cell Signaling Technology) and the supernatants were collected. Total protein content was measured using the Bradford assay (Bio-Rad). Lysates were incubated with protein-G–Sepharose beads (Santa Cruz Biotechnology) and anti–HIF-1α Ab (BD Biosciences) overnight and were then spun down for 1 minute at 5800*g*. The supernatant was removed and the pellets were solubilized with 6 × SDS sample buffer (0.35M Tris-HCl, pH 6.8, 10% SDS, 30% glycerol, 9.3% DTT) and analyzed by immunoblot analysis.

Immunoblotting. Cells were lysed with lysis buffer (Cell Signaling Technology) according to the manufacturer's instructions. The supernatants were collected, and total protein content was measured using the Bradford assay (Bio-Rad). The subcellular proteome extraction kit (Merck) was used to fractionate subcellular proteins. Lysates were separated by SDS-PAGE, transferred to a PVDF membrane, subjected to immunoblotting using anti–FIH-1 (1:200; Santa Cruz Biotechnology), anti-integrinβ1 (1/1000; Chemicon), and anti-α/β tubulin (1:1000; Cell Signaling Technology), washed with TBS-T, and immunoprobed for 1 hour at room temperature with HRP-conjugated or alkaline phosphatase–conjugated Ab, then washed with PBS-T. Finally, membranes were incubated with ECL-Plus (Amersham), and the chemiluminescent signal was detected using LAS4000 (Fujifilm) according to the manufacturer's instructions. The alkaline phosphatase signal was then detected using the Histofine Kit (Nichirei).

Immunoassay. After cell transfection with siRNA, the growth medium was replaced and the cells were cultured for 48 hours. Supernatants were then collected and analyzed for murine KitL, SDF-1α, and IL-7 using commercially available ELISAs (R&D Systems).

Stromal-based expansion cultures. A total of 1×10^4 Lin^- cells from the BM of GFP mice were cocultured with a confluent layer of stromal cells (MS-5). Recombinant mouse KitL (20 ng/mL, every other day) or recombinant mouse SDF-1α (100 ng/mL, every other day) was added to MT1-MMP KD MS-5 and control MS-5 cell cultures. Twelve days later, adherent cells were retrieved using trypsin (Sigma-Aldrich) and pooled with the nonadherent cells. Hematopoietic cells (GFP positive) were counted.

Migration assay. Migration assays were performed in 24-well plates using 5-μm polycarbonate Transwell inserts (Costar). BM Lin^- cells were collected and isolated from normal adult mice. The cells were resuspended in X-vivo 15 (Lonza). MT1-$MMP^{+/+}$ and MT1-$MMP^{-/-}$ MEF culture supernatant was aliquoted (600-μL aliquots) into 24-well plates, which formed the bottom chamber, in the presence or absence of neutralizing Abs against mouse SDF-1 (R&D Systems). Lin^- cells derived from the BM cells of GFP mice (2×10^5 cells in 100 μL) were added into the Transwell insert (top chamber), and the cells were allowed to migrate through the porous bottom for 4 hours at 37°C. The number of cells that migrated into the lower chamber was determined using flow cytometry. Cells had been stained with Abs against CD11b and Gr1 (BD Biosciences). The medium from the lower chamber was passed through a FACSCalibur for 60 seconds, gating on forward (FSC) and side scatter to exclude cell debris. The number of live cells was compared with a 100% migration control in which 2×10^5 cells had been added directly into the lower chamber and then counted on the FACScalibur for 60 seconds.

Immunohistochemistry. BM sections were fixed with 4% paraformaldehyde and permeabilized using 0.2% Triton X-100 for 20 minutes. After blocking in PBS containing 5% goat serum and 0.2% BSA, the sections were incubated with anti–FIH-1 Ab (Novus Biologicals) for 16 hours, washed 3 times with PBS and incubated for 1 hour with anti–rabbit Alexa 568 (Invitrogen). After washing, the sections were incubated with Alexa 488–conjugated nestin Ab (Abcam) for 2 hours. For HIF-1 staining, fixed and blocked sections were incubated with Alexa 488–conjugated HIF-1 Ab (BD Pharmingen) for 2 hours. The sections were mounted using Vectashield Mounting Medium with DAPI (Vector Laboratories). Images were acquired with an Olympus DP71 camera.

Micro-CT analysis. We evaluated the BM shaft surface area by using micro-CT (Rigaku). We measured the shaft area at the center of the femur by NIH ImageJ software.

Proliferation assay. A total of 2×10^4 Lin^- cells isolated by MACS (Miltenyi Biotec) from BM cells of GFP mice were cocultured with a confluent layer of MEF cells. The cells were maintained in X-vivo 15 supplemented recombinant mouse IL-3 (20 ng/mL, every other day) with or without neutralizing Abs against mouse KitL (R&D Systems). One week later, all cells were retrieved using trypsin (Sigma-Aldrich). GFP-positive were counted using FACS.

Statistical analysis

Data were analyzed using the unpaired 2-tailed Student *t* test and are expressed as means ± SEM. *P* values of $< .05$ were considered significant.

Results

MT1-MMP deletion leads to severe pancytopenia

We used 14-day-old MT1-$MMP^{-/-}$ mice to explore the role of MT1-MMP in the regulation of postnatal hematopoiesis, as mortality of older MT1-$MMP^{-/-}$ mice is very high.[24,28] Compared with MT1-$MMP^{+/+}$ mice, the body weight of MT1-$MMP^{-/-}$ mice was decreased (7.22 ± 0.48 and 2.99 ± 0.05 g/mouse, respectively; $n = 5$, $P < .001$) and there was a decline in all hematopoietic lineages examined in MT1-$MMP^{-/-}$ animals, including WBCs (Figure 1A), PLTs (Figure 1B), and RBCs (Figure 1C) in the PB. MT1-$MMP^{-/-}$ hematopoietic femurs were smaller than MT1-$MMP^{+/+}$ femurs (Figure 1D). Under steady-state conditions, BM cellularity in MT1-MMP mice was decreased compared with MT1-$MMP^{+/+}$ mice (Figure 1E). We next analyzed the number of MSCs by flow cytometry. The frequency of PDGFRα$^+$/Sca1$^+$/CD45$^-$/Ter119$^-$ BM-derived MSCs and nestin$^+$ niche cells was lower in MT1-$MMP^{-/-}$ BM cells than in MT1-$MMP^{+/+}$ BM cells (Figure 1F).[31] Because the skeletal malformation described in MT1-$MMP^{-/-}$ mice could affect the intrafemural space where hematopoiesis occurs, the BM shaft surface area was determined by microcomputer tomography (microCT). The BM shaft surface area was reduced in MT1-$MMP^{-/-}$ femurs compared with MT1-$MMP^{+/+}$ mice (Figure 1G).

Histologic analysis of BM sections showed that MT1-$MMP^{-/-}$ mice exhibited a striking paucity of hematopoietic cells within the BM shaft and a reduction in the number of megakaryocytes, which are responsible for platelet production (Figure 1H-I).

We next examined HSCs and hematopoietic progenitor populations. In wild-type mice, MT1-MMP is expressed in primary BMMCs within the lineage-negative (Lin^-) cell fraction, which contains mostly hematopoietic progenitor cells and a small fraction of HSCs, and in BM stromal cells, including BM endothelial cells (BMEC-1), fetal osteoblasts (FOB), and fibroblast-like stromal cells (MS-5; Figure 1J-K). The absolute number of CFU cells (CFU-C; Figure 1L) and of more primitive progenitor populations within BM cells, including day-8 CFU-spleen (CFU-S; Figure 1M), CMPs, GMPs, and MEPs and HSC-enriched CD34$^-$c-Kit$^+$, Sca-1$^+$, Lin^- (KSL) cells were diminished in MT1-$MMP^{-/-}$ BMMCs. To determine the HSC content of the BM, we performed limiting-dilution competitive repopulation analysis using MT1-$MMP^{+/+}$ or MT1-$MMP^{-/-}$ BMMCs. There was a lower frequency, and a significantly reduced absolute number of competitive repopulation units (CRUs) per femur in MT1-$MMP^{-/-}$ BMMCs than in MT1-$MMP^{+/+}$ BMMCs. These data indicate that MT1-MMP is required for HSC maintenance and for normal hematopoietic differentiation.

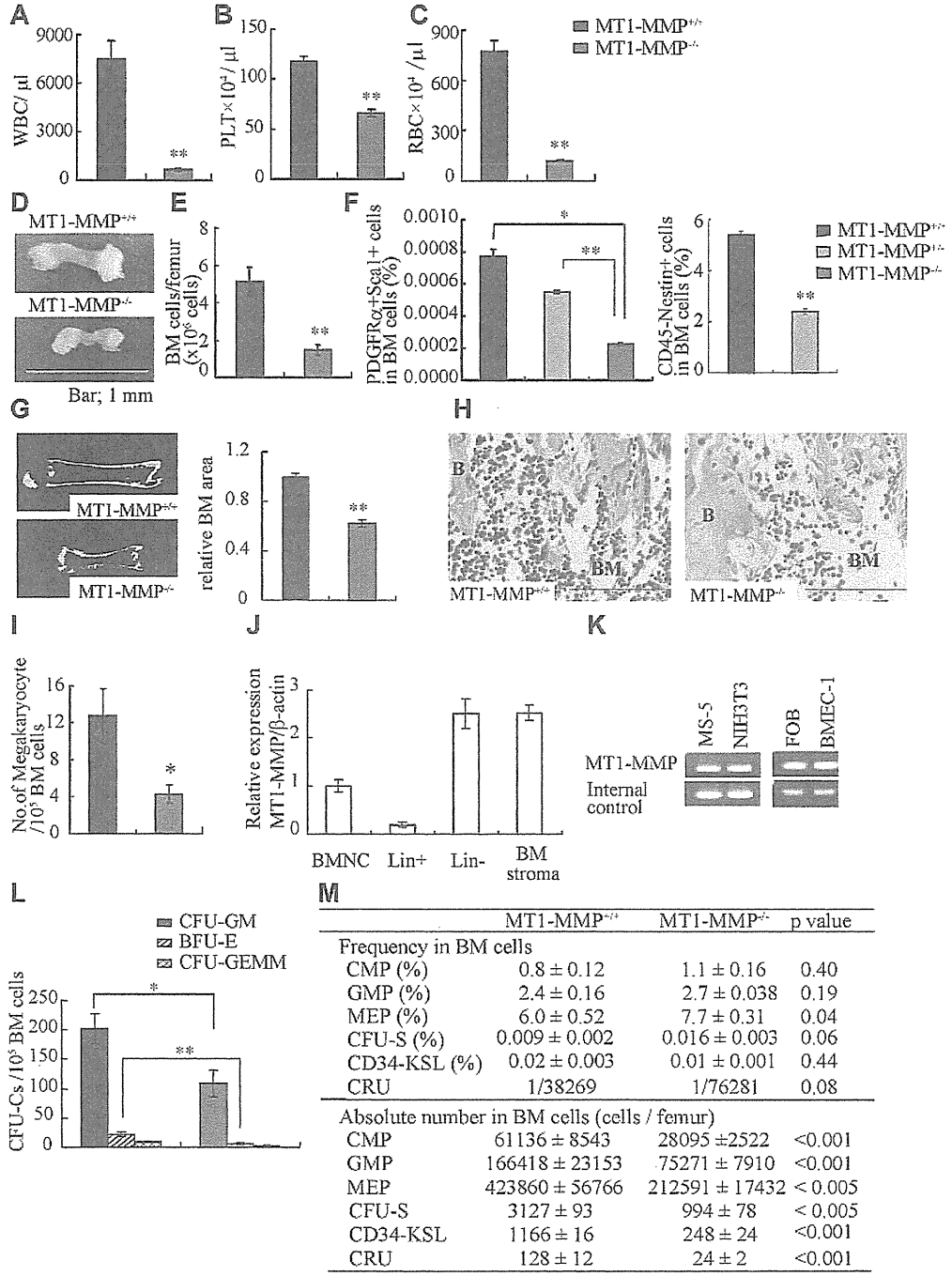

M

	MT1-MMP$^{+/+}$	MT1-MMP$^{-/-}$	p value
Frequency in BM cells			
CMP (%)	0.8 ± 0.12	1.1 ± 0.16	0.40
GMP (%)	2.4 ± 0.16	2.7 ± 0.038	0.19
MEP (%)	6.0 ± 0.52	7.7 ± 0.31	0.04
CFU-S (%)	0.009 ± 0.002	0.016 ± 0.003	0.06
CD34-KSL (%)	0.02 ± 0.003	0.01 ± 0.001	0.44
CRU	1/38269	1/76281	0.08
Absolute number in BM cells (cells / femur)			
CMP	61136 ± 8543	28095 ±2522	<0.001
GMP	166418 ± 23153	75271 ± 7910	<0.001
MEP	423860 ± 56766	212591 ± 17432	< 0.005
CFU-S	3127 ± 93	994 ± 78	< 0.005
CD34-KSL	1166 ± 16	248 ± 24	<0.001
CRU	128 ± 12	24 ± 2	<0.001

Figure 1. MT1-MMP gene deletion causes myelosuppression. (A-C) The number of (A) WBCs, (B) platelets (PLT), and (C) RBCs in the PB of 14-day-old mice was counted (n = 8). (D) Images of mouse femurs (bars, 1 mm). (E) Total BM cell number per femur. (F) The percentage of PDGFRα$^+$Sca1$^+$ cells (MSCs) was determined by flow cytometry (n = 2). (G) (left panel) Representative MicroCT scan images, and (right panel) quantification of the relative BM area within the BM femur shaft are presented (n = 3). (H) H&E-stained femur sections. Right panel shows the quantification of the BM area per femur. B indicates bone, (bars, 200 μm). (I) Megakaryocyte number (n = 5). (J-K) Real-time PCR analysis of MT1-MMP expression in (J) BM nuclear cells (BMNCs), Lin$^+$, Lin$^-$, and BM stroma cells, and (K) in MS-5, NIH3T3, FOB, and BMEC-1 cells. (L-M) The (L) absolute number of CFU-C per 10^5 BM cells and (M) frequency and absolute number/femur of CFU-S, CMP, GMP, MEP, CD34-KSL cells, and competitive repopulating units (CRU) in wild-type and knockout BM cells (n = 3). For CRU determination, freshly isolated BM cells of different cell concentration were transplanted into recipients (n = 10). Four months posttransplantation, the repopulating unit (RU) with trilineage engraftment (> 1% of donor-derived cells) was calculated. The absolute number of CRU was calculated based on the observed number of BM cells per femur. Errors in bar graphs are SEM; *$P < .05$, **$P < .01$. CFU-C indicates CFU cells; CFU-S, CFU-spleen; CMP, common myeloid progenitor; GMP, granulocyte/macrophage lineage-restricted progenitor; and MEP, megakaryocyte/erythrocyte lineage-restricted progenitor.

MT1-MMP$^{-/-}$ mice show a T- and B-cell differentiation defect

Compared with MT1-MMP$^{+/+}$ mice, the absolute numbers of PB CD3$^+$ T and B220$^+$ B lymphocytes were reduced (Figure 2A) and the spleen was much smaller (Figure 2B) in MT1-MMP$^{-/-}$ mice. Similar to the BM, histologic examination revealed less megakaryocytes in the MT1-MMP$^{-/-}$ spleen (Figure 2C). The white pulp appeared smaller in MT1-MMP$^{-/-}$ spleens (Figure 2C), which correlated with a reduction in the absolute numbers of lymphoid

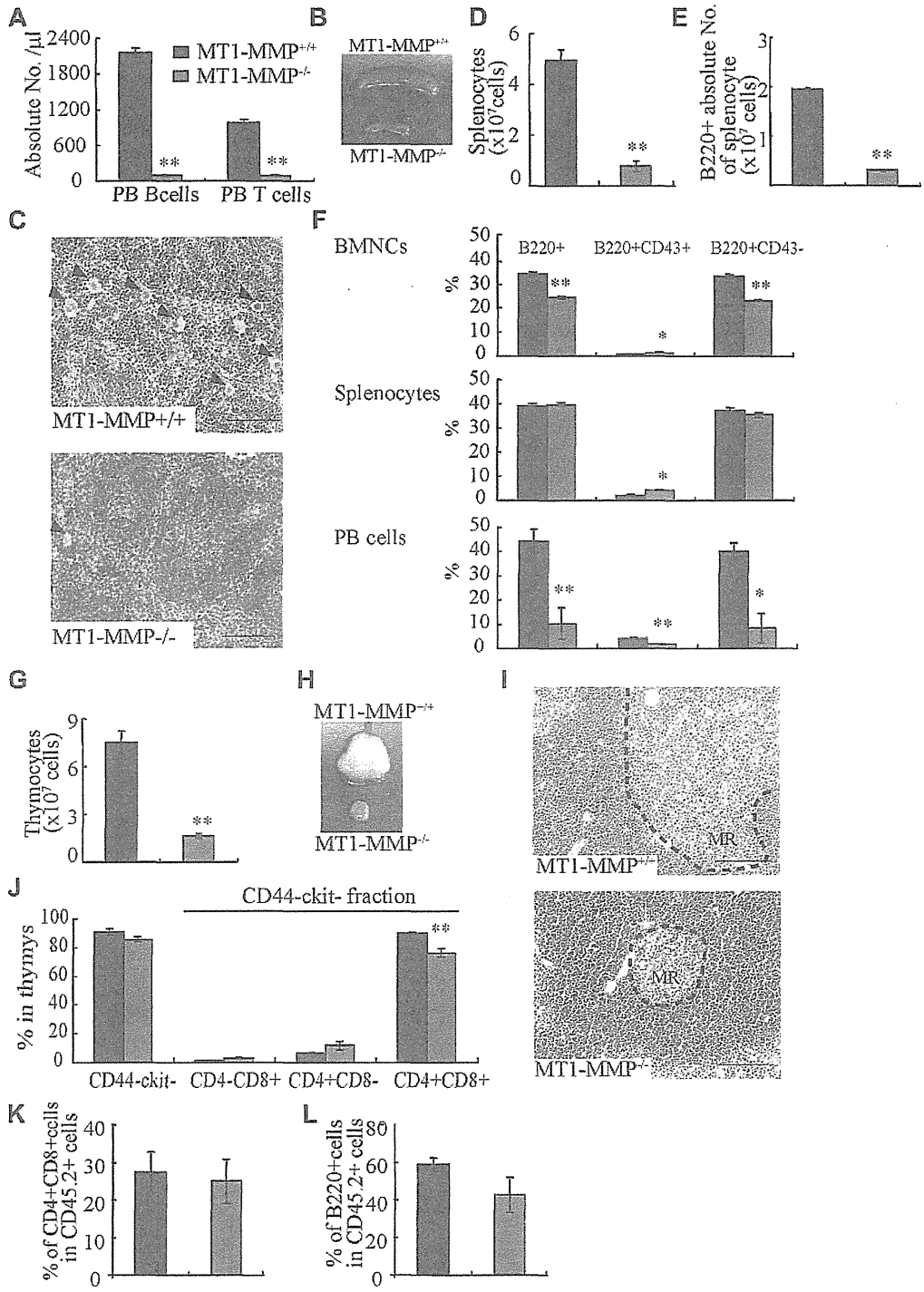

Figure 2. T and B lymphopoiesis are impaired in MT1-MMP$^{-/-}$ mice. (A) PB B- and T-cell numbers (FACS analysis). (B) Images of mouse spleens. (C) H&E-stained spleen sections. Arrowheads indicate megakaryocytes (bars, 100 μm). (D-E) The (D) total number of splenocytes and (E) B220$^+$ cells in splenocytes (n ≥ 6). (F) The percentage of B220$^+$ populations in BMNCs (n = 6), splenocytes (n = 3), and PB cells (n = 2). (G) Thymocyte number (n = 4). (H) Images of thymi. (I) H&E-stained thymus sections. MR indicates medullar region (bars, 100 μm). (J) The percentage of thymic T-lineage subpopulations. (K-L) BM cells from MT1-MMP$^{+/+}$ and MT1-MMP$^{-/-}$ mice were transplanted into wild-type animals (CD45.2). (K) The percentage of donor CD4$^+$/CD8$^+$ T and (L) B220$^+$B cell lineage contribution of donor-derived cells in the PB 4 months after transplantation (n = 10/group). Errors in bar graphs are SEM; *$P < .05$, **$P < .01$.

and total B (B220$^+$) spleen cells (Figure 2D-E). The percentage of B220$^+$, early- (B220$^+$CD43$^+$), and late-stage (B220$^+$CD43$^-$) B cells was reduced in MT1-MMP$^{-/-}$ BM, spleen, and PBMCs (Figure 2F). Although the absolute number of early- and late-stage B cells in splenocytes was reduced in MT1-MMP$^{-/-}$ mice (data not shown), the relative percentage of early (B220$^+$CD43$^+$) B cells was augmented in MT1-MMP$^{-/-}$ splenocytes. These data demonstrate that MT1-MMP is required for normal terminal B-cell differentiation within the BM with impaired release of B cells into the circulation.